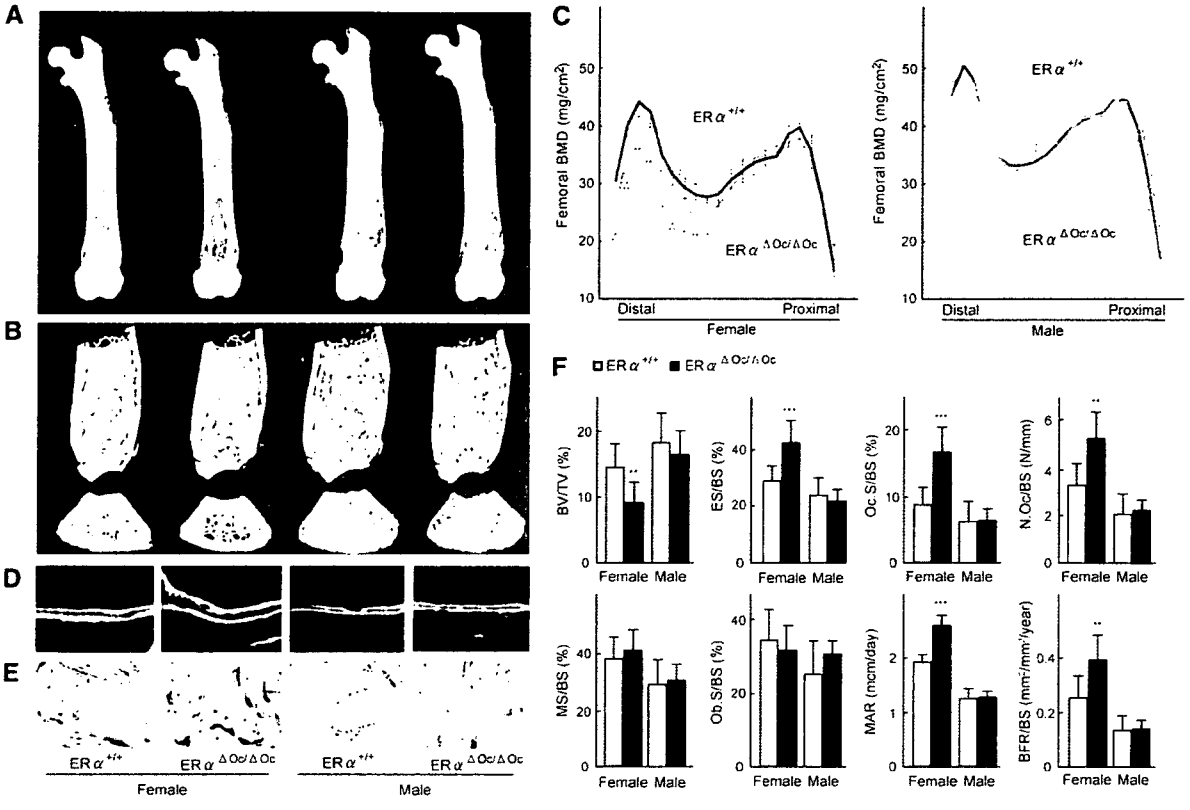

Figure 2. High Bone Turnover Osteopenia Was Observed in $ER\alpha^{\Delta Oc/\Delta Oc}$ Females But Not Males

(A) Soft X-ray images of femurs from 12-week-old $Ctsk^{Cre/+}$; $ER\alpha^{flox/flox}$ ($ER\alpha^{\Delta Oc/\Delta Oc}$) mice.

(B) Three-dimensional computed tomography images of the distal femurs and axial sections of distal metaphysis from representative 12-week-old $Ctsk^{Cre/+}$; $ER\alpha^{+/+}$ ($ER\alpha^{+/+}$) and $ER\alpha^{\Delta Oc/\Delta Oc}$ mice.

(C) BMD of each of 20 equal longitudinal divisions of femurs from 12-week-old $ER\alpha^{+/+}$ and $ER\alpha^{\Delta Oc/\Delta Oc}$ mice. (n = 10–11 animals per genotype; Student's t test, $^*p < 0.05$; $^{**}p < 0.01$; $^{***}p < 0.001$). Data are represented as mean ± SEM.

(D) Bone formation was also accelerated in $ER\alpha^{\Delta Oc/\Delta Oc}$ females when two calcein-labeled mineralized fronts visualized by fluorescent micrography were measured in the proximal tibia of 12-week-old mice.

(E) The number of TRAP-positive osteoclasts in the lumbar spine of female mice was increased by selective disruption of ERα in osteoclasts, indicating enhanced bone resorption.

(F) Bone turnover parameters as measured by dynamic bone histomorphometry after calcein labeling indicated high bone turnover in $ER\alpha^{\Delta Oc/\Delta Oc}$ females. Parameters are measured in the proximal tibia of 12-week-old $ER\alpha^{+/+}$ (open column) and $ER\alpha^{\Delta Oc/\Delta Oc}$ (filled column) mice. BV/TV: bone volume per tissue volume. ES/BS: eroded surface per bone surface. Oc.S/BS: osteoclast surface per bone surface. N.Oc/BS: osteoclast number per bone surface. MS/BS: mineralizing surface per bone surface. Ob.S/BS: osteoblast surface per bone surface. MAR: mineral apposition rate. BFR/BS: bone formation rate per bone surface (n = 10–11 animals per genotype; Student's t test, $^*p < 0.05$; $^{**}p < 0.01$; $^{***}p < 0.001$). Data are represented as mean ± SEM.

ERα protein expresses in differentiated osteoclasts in the bone tissues of femur sections from 12-week-old mice. ERα protein expression appeared abundant in osteoblasts and osteocytes of femur sections (Figure 4C) as well as hypothalamus (Figure S2B) from 12-week-old mice, in agreement with a previous report (Zaman et al., 2006). Likewise, expression levels of ERα in primary cultured osteoblasts derived from calvaria of $ER\alpha^{\Delta Oc/\Delta Oc}$ females appeared unaffected (Figure S2C). In contrast, in differentiated osteoclasts of the same femur sections, ERα expression was definitely detectable but very low in the $ER\alpha^{+/+}$ but undetectable in $ER\alpha^{\Delta Oc/\Delta Oc}$ females (Figure 4C).

Signaling by Osteoclastogenic Factors and Osteoclastogenesis Is Intact in Osteoclasts Deficient in ERα

It is possible that the osteoprotective function of osteoclastic ERα inhibits osteoclastogenesis. To address this issue, osteoclastogenesis was tested in cultured osteoclasts derived from bone-marrow cells of $ER\alpha^{\Delta Oc/\Delta Oc}$ mutants. In this cell culture system, a possible contribution of contaminated immune cells and stromal cells could be excluded, since osteoclastogenesis is only inducible by M-CSF treatment followed by M-CSF + RANKL (Koga et al., 2004).

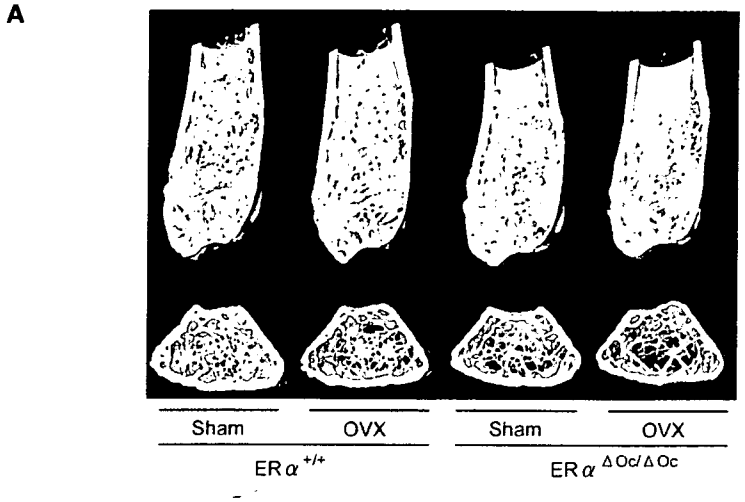

Oc.S/BS	8.31±1.6	11.0±0.3*	10.83±2.1*	10.53±0.5*
N.Oc/B.Pm	3.50±0.7	4.23±0.2*	4.28±0.6*	3.82±0.1*

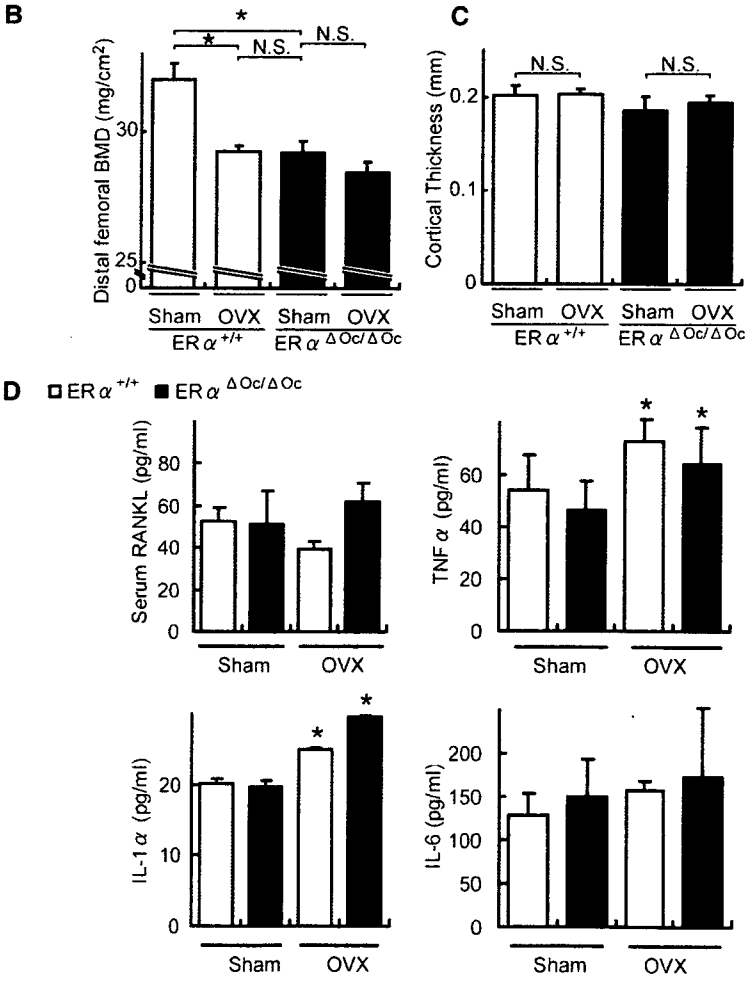

Figure 3. No Further Bone Loss of $ER\alpha^{\Delta Oc/\Delta Oc}$ Females by Ovariectomy

(A) Distal femoral micro CT analysis and lumbar vertebral bone histomorphometrical analysis of sham-operated or ovariectomized (OVX) 12-week-old $ER\alpha^{+/+}$ and $ER\alpha^{\Delta Oc/\Delta Oc}$ mice (*$p < 0.05$ compared to $ER\alpha^{+/+}$ sham group). Two weeks after OVX, the bone phenotype was analyzed.

(B) BMD of the distal femurs within each group are described in Figure 3A (*$p < 0.05$; N.S., not significant). Data are represented as mean ± SEM.

(C) Cortical thickness evaluation from micro CT analysis of femurs within each group described in Figure 3A. Data are represented as mean ± SEM.

(D) The levels of TNFα, IL-1α, and IL-6 in the bone-marrow cells culture media and serum RANKL (*$p < 0.05$ compared to each sham group). Data are represented as mean ± SEM.

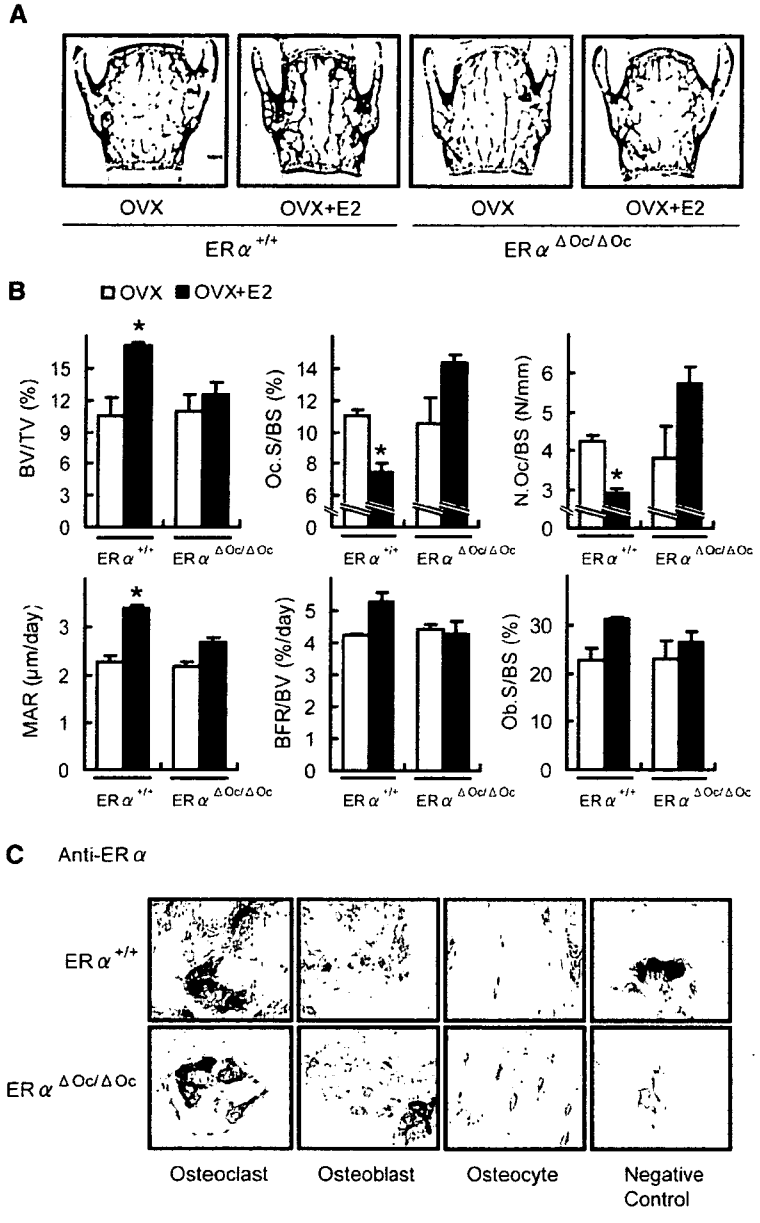

Figure 4. Estrogen treatment failed to reverse trabecular bone loss of ovariectomized $ER\alpha^{\Delta Oc/\Delta Oc}$ females

(A) von kossa staining of lumbar vertebral bodies of ovariectomized $ER\alpha^{+/+}$ and $ER\alpha^{\Delta Oc/\Delta Oc}$ mice treated with or without 17β-estradiol (0.83 μg/day) for 2 weeks (+E2) groups.

(B) Bone histomorphometrical analyses of the lumber vertebral bodies of 12-week-old ovariectomized $ER\alpha^{+/+}$ (left columns) and $ER\alpha^{\Delta Oc/\Delta Oc}$ (right columns) mice with (filled columns) or without (open columns) E2 treatment for 2 weeks (*$p < 0.05$ compared with E2-treated ovariectomized $ER\alpha^{\Delta Oc/\Delta Oc}$ mice). BV/TV: bone volume per tissue volume. ES/BS: eroded surface per bone surface. Oc.S/BS: osteoclast surface per bone surface. N.Oc/BS: osteoclast number per bone surface. MS/BS: mineralizing surface per bone surface. Ob.S/BS: osteoblast surface per bone surface. MAR: mineral apposition rate. BFR/BS: bone formation rate per bone surface. Data are represented as mean ± SEM.

(C) Immunochemical identification of ERα (brown) in TRAP-positive (red) differentiated osteoclasts. The femurs of 12 week-old mice were used for the immunodetection of ERα in bone cells. All labels were abolished when the primary antibody was preadsorbed with the immunizing peptide (negative control).

The number of TRAP-positive osteoclasts differentiated from the bone-marrow cells of $ER\alpha^{\Delta Oc/\Delta Oc}$ females was almost the same as that from $ER\alpha^{+/+}$ females (Figure 5A) and males (data not shown). The differentiated $ER\alpha^{\Delta Oc/\Delta Oc}$ osteoclasts had typical osteoclastic features, including the characteristic cell shape, TRAP-positive, multiple nuclei, and actin-ring formation, and were indistinguishable from the $ER\alpha^{+/+}$ osteoclasts (Figure 5B).

The expression levels of the prime osteoclastogenic transcription factors, c-*fos* and *NFATc1*, were unaltered by ERα deficiency in differentiated osteoclasts (Figure 5C). Furthermore, responses to RANKL in intracellular signaling, as represented by phosphorylation of p38 and IκB, were unaffected in $ER\alpha^{\Delta Oc/\Delta Oc}$ osteoclasts from females (Figure 5D) as well as males (data not shown). In light of these findings, it is unlikely that activated ERα in osteoclastic cells attenuates osteoclastogenesis.

Activation of the Fas/FasL System by Estrogen in Intact Bone Is Impaired by Osteoclastic ERα Deficiency

To examine osteoclastic ERα function in intact bone, DNA microarray analysis following real-time RT-PCR of RNA from the femurs of ovariectomized $ER\alpha^{\Delta Oc/\Delta Oc}$ females treated with or without estrogen, was performed. During

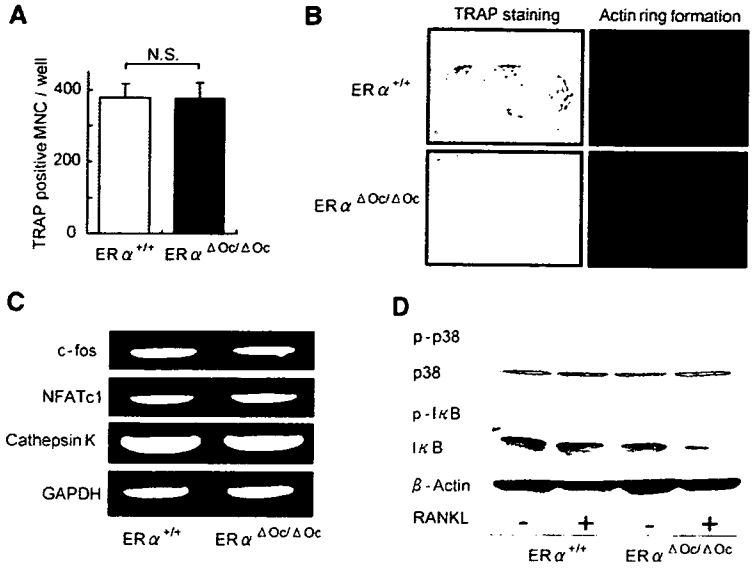

Figure 5. ERα Deficiency Did Not Affect Osteoclastogenesis

(A) TRAP-positive multinucleated cell count at 3 days after RANKL stimulation, cultured in 24-well plates (n = 6, N.S., not significant). Data are represented as mean ± SEM.

(B) TRAP staining and actin ring formation of RANKL induced primary cultured osteoclasts from bone-marrow cells of $ERα^{+/+}$ and $ERα^{ΔOc/ΔOc}$ mice.

(C) RT-PCR analysis of genes related to osteoclastogenesis.

(D) Western blot analysis of phosphorylated p38, JNK, and IκB of primary cultured bone-marrow cells stimulated with or without 100 ng/ml of RANKL for 15 min.

the search for candidate ERα target genes in bone by DNA microarray analysis (Figure S3), we found that a number of apoptosis-related factors were regulated by estrogen in the intact bone of $ERα^{+/+}$ females but dysregulated in $ERα^{ΔOc/ΔOc}$ females. This observation is consistent with a previous report of estrogen-induced apoptosis of mature osteoclasts (Kameda et al., 1997). Real-time RT-PCR to validate the estrogen regulations of the candidate genes revealed that gene expression of *FasL*, an apoptotic factor, was responsive to E2 (Figure 6A). Estrogen treatment (+E2) indeed induced expression of FasL protein in bone of ovariectomized $ERα^{+/+}$, but this induction was not obvious in ovariectomized $ERα^{ΔOc/ΔOc}$ mice (Figures 6B and 6C). Reflecting FasL induction by estrogen, estrogen-induced apoptosis (as observed by the TUNEL assay) in TRAP-positive mature trabecular osteoclasts in the distal femurs of the $ERα^{+/+}$ mice was detected, but this E2 response was abolished in the $ERα^{ΔOc/ΔOc}$ mice (Figure 6D). Furthermore, in mice lacking functional FasL ($FasL^{gld/gld}$), neither enhanced bone resorption nor bone mass loss was induced by ovariectomy (Figures 6E and 6F).

Osteoclastic ERα Mediates Estrogen-Induced apoptosis by FasL

The expression level of ERα protein in differentiated osteoclasts derived from bone marrow cells was very low, but induction of *FasL* gene expression was also detectable in the cultured osteoclasts of $ERα^{+/+}$ females as well as males (Figure 7A). However, this E2 response was impaired in cultured osteoclasts from $ERα^{ΔOc/ΔOc}$ females (Figure 7A). It is notable that such responses are also induced by tamoxifen (Figure 7C), which is an osteoprotective SERM (Harada and Rodan, 2003). ERα overexpression augmented *FasL* gene expression in response to estrogen in cultured osteoclasts from $ERα^{ΔOc/ΔOc}$ females (Figure S4A). In primary cultured calvarial osteoblasts from females as well as males (Suzawa et al., 2003), *FasL* gene induction by E2 and tamoxifen was also seen; however, it was not accompanied by increased apoptosis (data not shown). Thus, it appears that estrogen-induced apoptosis in osteoclasts is mediated by FasL expression in osteoclasts in the trabecular bone areas, presumably as well as in osteoblasts in cortical bone areas. As expected, the cell number of TUNEL-positive osteoclasts was increased by E2 in the cultured osteoclasts from $ERα^{+/+}$ females, but E2-induced apoptosis was undetectable in $ERα^{ΔOc/ΔOc}$ osteoclasts (Figure 7B). Consistent with FasL-induced apoptosis, *Fas* gene expression was observed (Figure 7D), but it was likely that Fas expression did not require ERα function (Figures S4B and S4C). Expression levels of *Fas* and *ERα* as well as E2 response in apoptosis appeared to fluctuate during osteoclast differentiation (Figures S4B–S4D); however, in FasL mutant ($FasL^{gld/gld}$) females, the E2-induced apoptosis was abolished (Figure S4E). These findings suggest that activated ERα in differentiated osteoclasts induces apoptosis through activating FasL/Fas signaling. This leads to suppression of bone resorption through truncating the already short life span of differentiated osteoclasts (Teitelbaum, 2006).

DISCUSSION

Selective ablation of ERα in mature osteoclasts in female mice shows that the osteoprotective effect of estrogen is mediated by osteoclastic ERα, at least in the trabecular regions of the tibiae, femur, and lumbar vertebrae of female mice. Activated ERα by estrogen as well as SERMs appears to truncate the already short life span (estimated at 2 weeks) of differentiated osteoclasts by inducing apoptosis through activation of the Fas/FasL system.

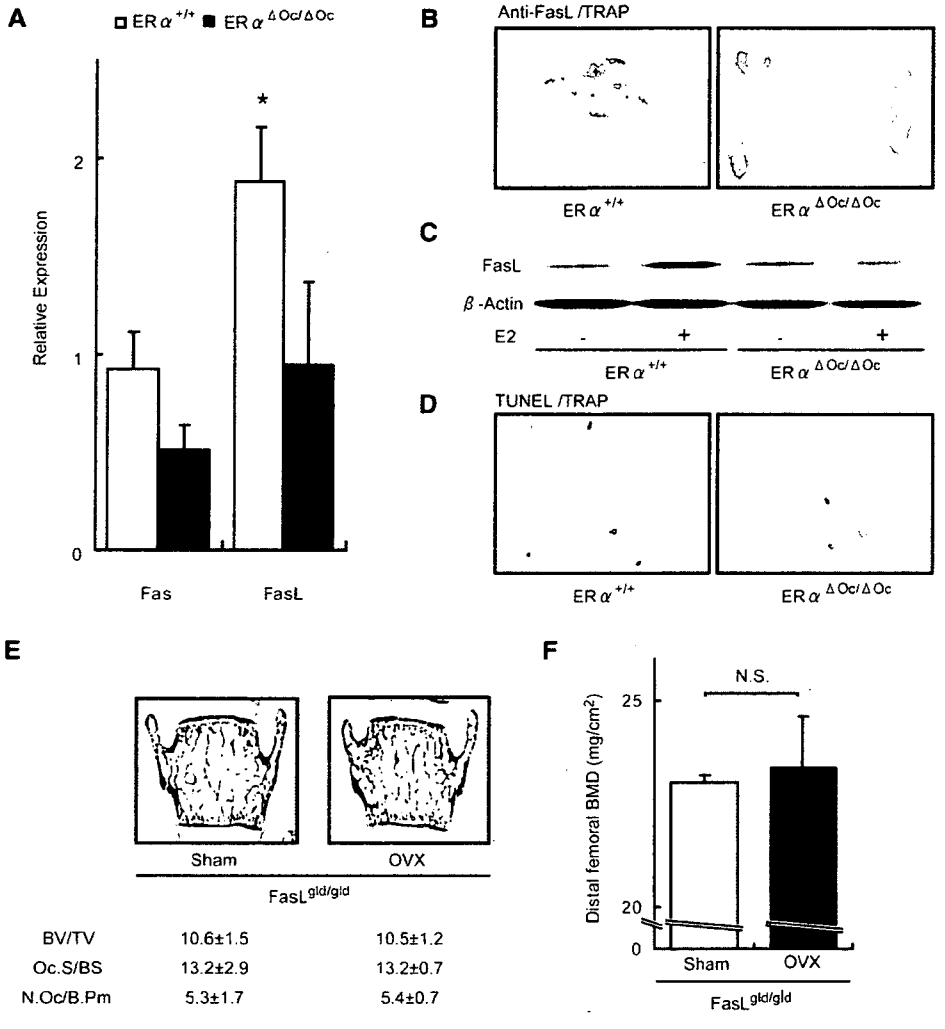

Figure 6. Activated ERα Induced Fas Ligand Expression and Apoptosis in Differentiated Osteoclasts of Intact Bone

(A) Real-time RT-PCR analysis of *Fas* and *FasL*. Expression levels in bones from E2-treated ovariectomized $ER\alpha^{+/+}$ (open column) and $ER\alpha^{\Delta Oc/\Delta Oc}$ (filled column) were compared with the ovariectomized groups of each genotype without E2 administration (*$p < 0.05$ compared to $ER\alpha^{+/+}$). Data are represented as mean ± SEM.

(B) Immunohistochemical analysis of anti-FasL with TRAP staining of the sections from the distal femurs of E2-treated ovariectomized $ER\alpha^{+/+}$ and $ER\alpha^{\Delta Oc/\Delta Oc}$ mice. Brawny stained cells are anti-FasL positive.

(C) Anti-FasL western blot analysis of proteins obtained from femurs of ovariectomized $ER\alpha^{+/+}$ and $ER\alpha^{\Delta Oc/\Delta Oc}$ mice treated with or without E2, using anti-β-actin as internal control.

(D) TUNEL staining with TRAP staining of the sections from the distal femurs of E2-treated ovariectomized $ER\alpha^{+/+}$ and $ER\alpha^{\Delta Oc/\Delta Oc}$ mice. Arrowheads indicate both TUNEL (brown)- and TRAP-positive staining cells.

(E) Bone histomorphometrical analysis of sham-operated or ovariectomized $FasL^{gld/gld}$ mice.

(F) BMD of the distal femurs of sham operated or ovariectomized $FasL^{gld/gld}$ mice. Data are represented as mean ± SEM.

This attenuates bone resorption. This idea is supported by previous observations that estrogen deficiency following menopause or ovariectomy leads to high bone turnover, particularly in the trabecular areas, as bone is rapidly lost through enhanced resorption (Delmas, 2002; Tolar et al., 2004). Thus, estrogen treatment leads to recovery from osteopenia by reducing resorption (Delmas, 2002; Rodan and Martin, 2000), partly by the induction of osteoclast cell death.

In contrast to the osteopenia seen in the $ER\alpha^{\Delta Oc/\Delta Oc}$ females, the $ER\alpha^{\Delta Oc/\Delta Oc}$ male mice unexpectedly had no bone loss. The male mice still demonstrated an ERα-mediated induction of FasL in response to estrogen with subsequent apoptosis of osteoclasts (Figure 7). Both male mice with a deficiency of aromatase that are unable to locally produce estrogen from testosterone and men with a genetic mutation in the *ERα* gene suffer from osteoporosis (Smith et al., 1994). Considering that the

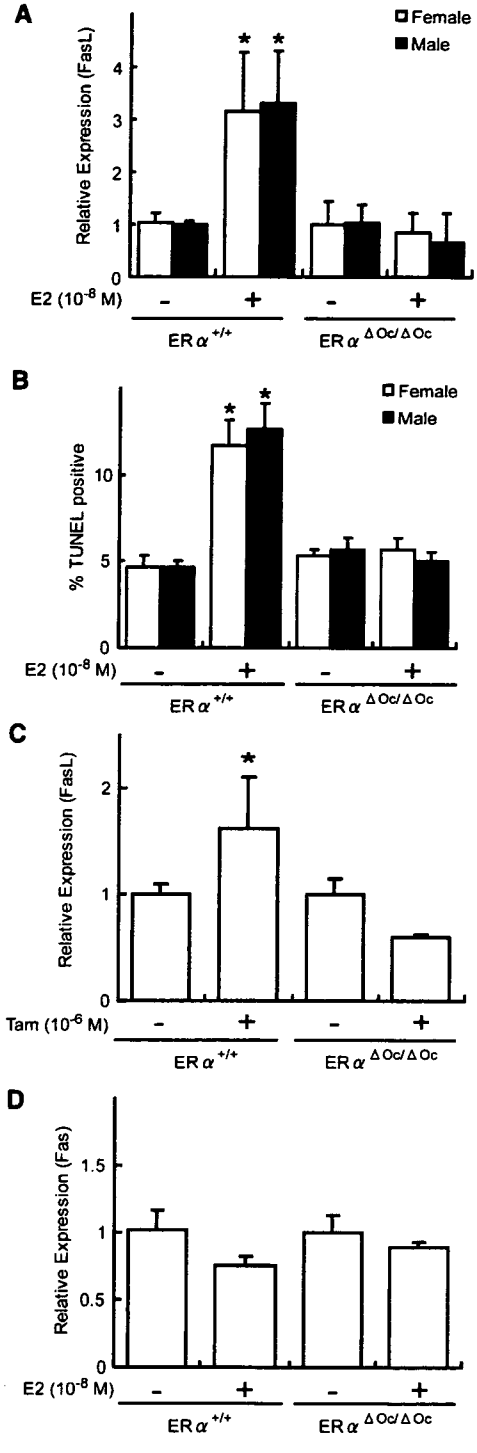

Figure 7. Estrogen-Induced *FasL* Expression and Apoptosis Required ERα in Cultured Osteoclasts

(A) Real-time RT-PCR analysis of *FasL* expression using total RNA obtained from in vitro primary cultured osteoclasts of each genotype at 3 days after RANKL stimulation, treated with or without E2 (10^{-8} M) for 4 hr (*$p < 0.05$ compared to the group treated without E2). Data are represented as mean ± SEM.

(B) Apoptotic cells were defined as those with TUNEL-positive nuclei among TRAP-positive multinucleated primary cultured osteoclasts treated with or without E2 (10^{-8} M) for 12 hr in 96-well plates (*$p < 0.05$ compared to the group treated without E2). Data are represented as mean ± SEM.

(C) *FasL* expression in each genotypic female osteoclastic cells treated with or without Tam (10^{-6} M) (*$p < 0.05$ compared to the group treated without Tam). Data are represented as mean ± SEM.

(D) Expression of *Fas* was measured as described in the legend of Figure 7A. Data are represented as mean ± SEM.

markedly elevated levels of testosterone in ERα KO females may be potent enough to maintain normal bone turnover (Syed and Khosla, 2005), it is likely that the activated AR might be functionally sufficient in male mice to compensate for the ERα deficiency in bone (Kawano et al., 2003). However, species differences in the osteoprotective action of sex steroid hormones still need to be carefully addressed.

Fas/FasL system-mediated apoptotic induction of osteoclasts by estrogen may well be a part of the mechanism for the antiresorptive action of estrogen and SERMs in trabecular bone areas (Delmas, 2002; Rodan and Martin, 2000; Simpson and Davis, 2001; Syed and Khosla, 2005; Tolar et al., 2004). Regulation of osteoclast differentiation is tightly coupled to osteoblastic function in terms of cytokine production and cell-cell contact (Karsenty and Wagner, 2002; Martin and Sims, 2005; Mundy and Elefteriou, 2006; Teitelbaum and Ross, 2003). Indeed, upregulation of osteoclastogenic cytokines by ovariectomy was unaffected in $ER\alpha^{\Delta Oc/\Delta Oc}$ females. Considering the observation that cortical bone mass is increased in ovariectomized $ER\alpha^{\Delta Oc/\Delta Oc}$ females during estrogen treatment, it is conceivable that the antiresorptive estrogen action in cortical bone is also mediated by osteoblastic ERα. In this regard, FasL induction by estrogen in osteoblasts may contribute to the osteoprotective estrogen action, and *FasL* gene induction by estrogen was in fact detected in primary cultured osteoblasts from female calvaria by us as well as another group (S. Krum and M. Brown, personal communication). Thus, similar experiments in which ERα is selectively ablated in osteoblasts are needed to define the role of ERα in these cells.

In osteoclastic cells, expression of the *FasL* gene, which leads to apoptosis, appears to be positive controlled by activated ERα. Not surprisingly, a direct binding site for ERα has been mapped in the *FasL* gene locus (S. Krum and M. Brown, personal communication). An osteoclast- and cell-differentiation stage-specific mechanism may underlie this gene induction in the *FasL* gene promoter. A recent study demonstrated that ERα recruitment to specific promoter sites of given ERα target genes was cell-type specific (Carroll et al., 2005). Thus, there is significant impetus to identify the osteoclastic factor that associates with ERα in the *FasL* gene promoter. Such identification will lead to a better understanding of the molecular basis of the osteoprotective estrogen action and provide a target against which to develop SERMs of greater effectiveness.

EXPERIMENTAL PROCEDURES

Ctsk-Cre Construction and Generation of the Knockin Mouse Lines

An RP23-422n18 BAC clone containing the mouse *Ctsk* gene was purchased from Invitrogen (Carlsbad, CA). The *FRT-Kan^r/Neo^r-FRT* and *nlsCre* fragments were obtained from plasmids pSK2/3-*FRT-Neo* and pIC-*Cre*. Two homologous arms of 500 bp from the *Ctsk* gene were inserted into both sides of the *nlsCre-FRT-Kan^r/Neo^r-FRT* cassette in the pSK2/3-*FRT-Neo* plasmid. The *nlsCre-FRT-Kan^r/Neo^r-FRT* cassette was introduced into the endogenous ATG start site of the *Ctsk* gene by recombineering approaches (Copeland et al., 2001). Targeted BAC was reduced in size from 189 kb to 26 kb and subcloned into the pMC1-DTpA vector by the gap-repair method. The targeted TT2 ES clones were selected after positive-negative selection with G418 and DT-A with Southern analysis, then aggregated with single eight-cell embryos from CD-1 mice (Yoshizawa et al., 1997). Chimeric mice were then crossed with a general deleter mouse line, *ACTB-Flpe* (Jackson Laboratory), to remove the *Kan^r/Neo^r* cassette. The *Ctsk-Cre* mice (*Ctsk$^{Cre/+}$*), originally on a hybrid C57BL/6 and CBA genetic background, were backcrossed for four generations into a C57BL/6J background. *FasL$^{gld/gld}$* mice were also purchased from Jackson Laboratory.

Analysis of Cre Recombinase Activities

Expression of the Cre transcript was detected by RT-PCR. Southern analysis using a *Cre* cDNA probe was performed with total RNA extracted from 12-week-old mice. To evaluate the specificity and efficiency of Cre-mediated recombination, we mated the *Ctsk$^{Cre/+}$* mice to *CAG-CAT-Z* reporter mice (kindly provided by J. Miyazaki) (Sakai and Miyazaki, 1997) and genotyped their offspring with *Cre*-specific primers. β-galactosidase activity of the expressed *LacZ* gene driven by the *CAG* promoter was expected to be detected in the given cells expressing functional Cre recombinase.

In Vitro Osteoclastogenesis and Ligand Application

Bone-marrow cells derived from 8-week-old mice were plated in culture dishes containing α-MEM (GIBCO-BRL) with 10% FBS (JRH) and 10 ng/ml M-CSF (Genzyme). After incubation for 48 hr, adherent cells were used as osteoclast precursor cells after washing out the nonadherent cells. Cells were cultured in the presence of 10 ng/ml M-CSF and 100 ng/ml RANKL (Peprotech) to generate osteoclast-like cells (Koga et al., 2004) for 3 days, so the total culture time was 5 days. Three days after RANKL stimulation, primary cultured osteoclasts were treated with 10^{-8} M of 17β-estradiol (E2) (Sigma-Aldrich Co.) or 10^{-6} M 4-hydroxytamoxifen (Tam) (Sigma-Aldrich Co.) in phenol-red free medium.

Generation of Osteoclast-Specific ERα KO Mice

The ERα conditional (*ERα$^{flox/flox}$*) (Dupont et al., 2000) and null alleles with a C57BL/6J background have been previously described. *ERα$^{flox/flox}$* mice were crossed with *Ctsk$^{Cre/+}$* mice to generate *Ctsk$^{Cre/+}$; ERα$^{flox/+}$* mice. *Ctsk$^{Cre/+}$; ERα$^{+/+}$* (*ERα$^{+/+}$*) and *Ctsk$^{Cre/+}$; ERα$^{flox/flox}$* (*ERα$^{ΔOc/ΔOc}$*) mice were obtained by crossing *Ctsk$^{Cre/+}$; ERα$^{flox/+}$* with *ERα$^{flox/+}$* mouse lines.

Radiological Analysis

Bone radiographs of the femurs of 12-week-old *Ctsk$^{Cre/+}$; ERα$^{flox/flox}$* (*ERα$^{ΔOc/ΔOc}$*) and *Ctsk$^{Cre/+}$; ERα$^{+/+}$* (*ERα$^{+/+}$*) littermates were visualized with a soft X-ray apparatus (TRS-1005: SOFTRON). BMD was measured by DXA using a bone mineral analyzer (DCS-600EX: ALOKA). Micro Computed Tomography scanning of the femurs was performed using a composite X-ray analyzer (NX-CP-C80H-IL: Nittetsu ELEX Co.) (Kawano et al., 2003). Tomograms were obtained with a slice thickness of 10 μm and reconstructed at 12 × 12 pixels into a 3D image by the volume-rending method (VIP-Station; Teijin System Technology) using a computer.

Analysis of Skeletal Morphology

Twelve-week-old *Ctsk$^{Cre/+}$; ERα$^{flox/flox}$* (*ERα$^{ΔOc/ΔOc}$*) and *Ctsk$^{Cre/+}$; ERα$^{+/+}$* (*ERα$^{+/+}$*) littermates were double labeled with subcutaneous injections of 16 mg/kg of calcein (Sigma) at 4 and 2 days before sacrifice. Tibiae were removed from each mouse and fixed with 70% ethanol. They were stained with Villanueva bone stain for 7 days and embedded in methyl-methacrylate (Wako) (Yoshizawa et al., 1997). Frontal plane sections (5-μm thick) of the proximal tibia were cut using a Microtome (LEICA). The cancellous bone was measured in the secondary spongiosa located 500 μm from the epiphyseal growth plate and 160 μm from the endocortical surface (Kawano et al., 2003; Nakamichi et al., 2003). Bone histomorphometric measurements of the tibia were made using a semiautomatic image analyzing system (System Supply) and a fluorescent microscope (Optiphot; Nikon). Similar measurements of the lumbar vertebral bodies were done as previously reported (Takeda et al., 2002). Standard bone histomorphometrical nomenclatures, symbols, and units were used as described in the report of the ASBMR Histomophometry Nomenclature Committee.

Ovariectomy and Hormone Replacement

Female *Ctsk$^{Cre/+}$; ERα$^{flox/flox}$* (*ERα$^{ΔOc/ΔOc}$*) and *Ctsk$^{Cre/+}$; ERα$^{+/+}$* (*ERα$^{+/+}$*) littermates were ovariectomized or sham operated at 8–12 weeks of age for 2 weeks for all experiments, and slow releasing pellets of E2 (0.83 μg/day) or placebo (Innovative Research, Sarasota, FL) were implanted subcutaneously in the scapular region behind the neck (Sato et al., 2004; Shiina et al., 2006).

Immunohistochemistry

Twelve-week-old *Ctsk$^{Cre/+}$; ERα$^{flox/flox}$* (*ERα$^{ΔOc/ΔOc}$*) and *Ctsk$^{Cre/+}$; ERα$^{+/+}$* (*ERα$^{+/+}$*) littermates were fixed with 4% PFA by perfusion. Serial sections of the brain (20 μm thick) were divided into two groups and used for single labeling for the ERα or thionin to allow determination of the areas to be measured. Tibiae and femurs were decalcified in 10% EDTA for 2–4 weeks after fixation and then embedded in paraffin sections. Sections were incubated in L.A.B. solution (Polysciences) for 30 min to retrieve antigen. The cooled sections were incubated in 1% H_2O_2 for 30 min to quench endogenous peroxidase and then washed with 1% Triton X-100 in PBS for 10 min. To block nonspecific antibody binding, sections were incubated in blocking solution (DAKO) for 5 min. Sections were then incubated with anti-ERα (Santa Cruz, CA) and anti-FasL (Santa Cruz, CA) in blocking solution overnight at 4°C. Staining was then performed using the EnVision+ HRP System (Dako) and 3, 3′-diaminobendizine tetrahydrochloride substrate (Sigma), counterstained with TRAP, dehydrated through an ethanol series and xylene, before mounting (Sato et al., 2004).

ERα Overexpression

Two days after RANKL stimulation, an expression vector of mouse ERα was tranfected into immature osteoclastic cells from *ERα$^{ΔOc/ΔOc}$* mice using Superfect (QIAGEN) as manufacture's instruction.

Real-Time RT-PCR

One microgram of total RNA from each sample was reverse transcribed into first-strand cDNA with random hexamers using Superscript III reverse transcriptase (Invitrogen). Primer sets for all genes were purchased from Takara Bio. Inc. (Tokyo, Japan). Real-time RT-PCR was performed using SYBR Premix Ex Taq (Takara) with the ABI PRISM 7900HT (Applied Biosystems) according to the manufacturer's instructions. Experimental samples were matched to a standard curve generated by amplifying serially diluted products using the same PCR protocol. To correct for variability in RNA recovery and efficiency of reverse transcription, *Gapdh* cDNA was amplified and quantified in each cDNA preparation. Normalization and calculation steps were performed as reported previously (Takezawa et al., 2007).

TUNEL/TRAP Staining

The TUNEL method was performed using the ApopTag Fluorescein In Situ Apoptosis Detection Kit (CHEMICON international) according to the manufacturer's instructions with a slight modification. This was followed by TRAP staining as previously reported (Kobayashi et al., 2000).

Cytokine Assays

Bone marrow and blood were collected at 2 weeks after sham operation or ovariectomy. Bone-marrow cells were cultured for 3 days in DMEM. The levels of TNFα, IL-1α, and IL-6 in the culture media and serum RANKL were determined by ELISA (R&D Systems).

Western Blot

Osteoclast precursor cells were treated with or without 100 ng/ml of soluble RANKL. After 15 minutes, cell extracts were harvested from the cells using lysis buffer containing 100 mM Tris-HCl (pH 7.8), 150 mM NaCl, 0.1% Triton X-100, 5% protease inhibitor cocktail (Sigma), and 5% phosphatase inhibitor cocktail (Sigma). An equivalent amount of protein from each of the cell extracts and proteins of femoral bone extracted using ISOGEN was loaded for SDS-PAGE and transferred to PVDF membranes (Amersham Biosciences). The membranes were developed with enhanced chemiluminescence reagent (Amersham Biosciences) (Ohtake et al., 2003). Phosphorylation of p38 MAPK and IκB were evaluated using antibodies purchased from Cell Signaling Technology (Koga et al., 2004) and anti-FasL antibody was purchased from Santa Cruz Biotechnology (sc-834).

Actin-Ring Formation

Cells were fixed for 15 min in warm 4% paraformaldehyde (PFA). After fixation, cells were washed three times with PBS with 0.1% Triton X-100 (PBST) and incubated with 0.2 U/ml rhodamine phalloidin (Molecular Probes) for 30 min and washed again three times in PBST.

Statistical Analysis

Data were analyzed by two-tailed student's t test. For all graphs, data are represented as mean ± SEM.

Supplemental Data

Supplemental Data include Supplemental Experimental Procedures and four figures and can be found with this article online at http://www.cell.com/cgi/content/full/130/5/811/DC1/.

ACKNOWLEDGMENTS

We thank Drs. S. Krum and M. Brown to share with their unpublished results; Drs. K. Yoshimura, Y. Nakamichi, T. Watanabe, J. Miyamoto, H. Shiina, T. Fukuda, Ms. Y. Sato, and S. Tanaka for generation of the KO mice; Drs. T. Koga, H. Takagi, E. Ochiai, and N. Moriyama for technical help; Dr. J. Miyazaki for *CAG-CAT-Z* reporter mice, and H. Higuchi and K. Hiraga for manuscript preparation. This work was supported in part by priority areas from the Ministry of Education, Culture, Sports, Science and Technology (to S.K.) and the Program for Promotion of Basic Research Activities for Innovative Biosciences (PROBRAIN).

Received: February 23, 2007
Revised: May 21, 2007
Accepted: July 17, 2007
Published: September 6, 2007

REFERENCES

Belandia, B., and Parker, M.G. (2003). Nuclear receptors: a rendezvous for chromatin remodeling factors. Cell *114*, 277–280.

Bland, R. (2000). Steroid hormone receptor expression and action in bone. Clin. Sci. (Lond.) *98*, 217–240.

Carroll, J.S., Liu, X.S., Brodsky, A.S., Li, W., Meyer, C.A., Szary, A.J., Eeckhoute, J., Shao, W., Hestermann, E.V., Geistlinger, T.R., et al. (2005). Chromosome-wide mapping of estrogen receptor binding reveals long-range regulation requiring the forkhead protein FoxA1. Cell *122*, 33–43.

Chien, K.R., and Karsenty, G. (2005). Longevity and lineages: toward the integrative biology of degenerative diseases in heart, muscle, and bone. Cell *120*, 533–544.

Copeland, N.G., Jenkins, N.A., and Court, D.L. (2001). Recombineering: a powerful new tool for mouse functional genomics. Nat. Rev. Genet. *2*, 769–779.

Couse, J.F., and Korach, K.S. (1999). Estrogen receptor null mice: what have we learned and where will they lead us? Endocr. Rev. *20*, 358–417.

Delmas, P.D. (2002). Treatment of postmenopausal osteoporosis. Lancet *359*, 2018–2026.

Dupont, S., Krust, A., Gansmuller, A., Dierich, A., Chambon, P., and Mark, M. (2000). Effect of single and compound knockouts of estrogen receptors alpha (ERalpha) and beta (ERbeta) on mouse reproductive phenotypes. Development *127*, 4277–4291.

Gowen, M., Lazner, F., Dodds, R., Kapadia, R., Feild, J., Tavaria, M., Bertoncello, I., Drake, F., Zavarselk, S., Tellis, I., et al. (1999). Cathepsin K knockout mice develop osteopetrosis due to a deficit in matrix degradation but not demineralization. J. Bone Miner. Res. *14*, 1654–1663.

Harada, S., and Rodan, G.A. (2003). Control of osteoblast function and regulation of bone mass. Nature *423*, 349–355.

Kameda, T., Mano, H., Yuasa, T., Mori, Y., Miyazawa, K., Shiokawa, M., Nakamaru, Y., Hiroi, E., Hiura, K., Kameda, A., et al. (1997). Estrogen inhibits bone resorption by directly inducing apoptosis of the bone-resorbing osteoclasts. J. Exp. Med. *186*, 489–495.

Karsenty, G. (2006). Convergence between bone and energy homeostases: leptin regulation of bone mass. Cell Metab. *4*, 341–348.

Karsenty, G., and Wagner, E.F. (2002). Reaching a genetic and molecular understanding of skeletal development. Dev. Cell *2*, 389–406.

Kato, S., Ito, S., Noguchi, T., and Naito, H. (1989). Effects of brefeldin A on the synthesis and secretion of egg white proteins in primary cultured oviduct cells of laying Japanese quail (Coturnix coturnix japonica). Biochim. Biophys. Acta *991*, 36–43.

Kawano, H., Sato, T., Yamada, T., Matsumoto, T., Sekine, K., Watanabe, T., Nakamura, T., Fukuda, T., Yoshimura, K., Yoshizawa, T., et al. (2003). Suppressive function of androgen receptor in bone resorption. Proc. Natl. Acad. Sci. USA *100*, 9416–9421.

Kimble, R.B., Matayoshi, A.B., Vannice, J.L., Kung, V.T., Williams, C., and Pacifici, R. (1995). Simultaneous block of interleukin-1 and tumor necrosis factor is required to completely prevent bone loss in the early postovariectomy period. Endocrinology *136*, 3054–3061.

Kobayashi, Y., Hashimoto, F., Miyamoto, H., Kanaoka, K., Miyazaki-Kawashita, Y., Nakashima, T., Shibata, M., Kobayashi, K., Kato, Y., and Sakai, H. (2000). Force-induced osteoclast apoptosis in vivo is accompanied by elevation in transforming growth factor beta and osteoprotegerin expression. J. Bone Miner. Res. *15*, 1924–1934.

Koga, T., Inui, M., Inoue, K., Kim, S., Suematsu, A., Kobayashi, E., Iwata, T., Ohnishi, H., Matozaki, T., Kodama, T., et al. (2004). Costimulatory signals mediated by the ITAM motif cooperate with RANKL for bone homeostasis. Nature *428*, 758–763.

Li, C.Y., Jepsen, K.J., Majeska, R.J., Zhang, J., Ni, R., Gelb, B.D., and Schaffler, M.B. (2006). Mice lacking Cathepsin K maintain bone remodeling but develop bone fragility despite high bone mass. J. Bone Miner. Res. *21*, 865–875.

Mangelsdorf, D.J., Thummel, C., Beato, M., Herrlich, P., Schutz, G., Umesono, K., Blumberg, B., Kastner, P., Mark, M., Chambon, P., and Evans, R.M. (1995). The nuclear receptor superfamily: the second decade. Cell *83*, 835–839.

Martin, T.J., and Sims, N.A. (2005). Osteoclast-derived activity in the coupling of bone formation to resorption. Trends Mol. Med. *11*, 76–81.

Mueller, S.O., and Korach, K.S. (2001). Estrogen receptors and endocrine diseases: lessons from estrogen receptor knockout mice. Curr. Opin. Pharmacol. *1*, 613–619.

Mundy, G.R., and Elefteriou, F. (2006). Boning up on ephrin signaling. Cell *126*, 441–443.

Nakamichi, Y., Shukunami, C., Yamada, T., Aihara, K., Kawano, H., Sato, T., Nishizaki, Y., Yamamoto, Y., Shindo, M., Yoshimura, K., et al. (2003). Chondromodulin I is a bone remodeling factor. Mol. Cell. Biol. *23*, 636–644.

Ohtake, F., Takeyama, K., Matsumoto, T., Kitagawa, H., Yamamoto, Y., Nohara, K., Tohyama, C., Krust, A., Mimura, J., Chambon, P., et al. (2003). Modulation of oestrogen receptor signalling by association with the activated dioxin receptor. Nature *423*, 545–550.

Raisz, L.G. (2005). Pathogenesis of osteoporosis: concepts, conflicts, and prospects. J. Clin. Invest. *115*, 3318–3325.

Riggs, B.L., and Hartmann, L.C. (2003). Selective estrogen-receptor modulators–mechanisms of action and application to clinical practice. N. Engl. J. Med. *348*, 618–629.

Rodan, G.A., and Martin, T.J. (2000). Therapeutic approaches to bone diseases. Science *289*, 1508–1514.

Saftig, P., Hunziker, E., Wehmeyer, O., Jones, S., Boyde, A., Rommerskirch, W., Moritz, J.D., Schu, P., and von Figura, K. (1998). Impaired osteoclastic bone resorption leads to osteopetrosis in Cathepsin-K-deficient mice. Proc. Natl. Acad. Sci. USA *95*, 13453–13458.

Sakai, K., and Miyazaki, J. (1997). A transgenic mouse line that retains Cre recombinase activity in mature oocytes irrespective of the cre transgene transmission. Biochem. Biophys. Res. Commun. *237*, 318–324.

Sato, T., Matsumoto, T., Kawano, H., Watanabe, T., Uematsu, Y., Sekine, K., Fukuda, T., Aihara, K., Krust, A., Yamada, T., et al. (2004). Brain masculinization requires androgen receptor function. Proc. Natl. Acad. Sci. USA *101*, 1673–1678.

Shang, Y., and Brown, M. (2002). Molecular determinants for the tissue specificity of SERMs. Science *295*, 2465–2468.

Shiina, H., Matsumoto, T., Sato, T., Igarashi, K., Miyamoto, J., Takemasa, S., Sakari, M., Takada, I., Nakamura, T., Metzger, D., et al. (2006). Premature ovarian failure in androgen receptor-deficient mice. Proc. Natl. Acad. Sci. USA *103*, 224–229.

Simpson, E.R., and Davis, S.R. (2001). Minireview: aromatase and the regulation of estrogen biosynthesis–some new perspectives. Endocrinology *142*, 4589–4594.

Sims, N.A., Clement-Lacroix, P., Minet, D., Fraslon-Vanhulle, C., Gaillard-Kelly, M., Resche-Rigon, M., and Baron, R. (2003). A functional androgen receptor is not sufficient to allow estradiol to protect bone after gonadectomy in estradiol receptor-deficient mice. J. Clin. Invest. *111*, 1319–1327.

Smith, E.P., Boyd, J., Frank, G.R., Takahashi, H., Cohen, R.M., Specker, B., Williams, T.C., Lubahn, D.B., and Korach, K.S. (1994). Estrogen resistance caused by a mutation in the estrogen-receptor gene in a man. N. Engl. J. Med. *331*, 1056–1061.

Sun, L., Peng, Y., Sharrow, A.C., Iqbal, J., Zhang, Z., Papachristou, D.J., Zaidi, S., Zhu, L.L., Yaroslavskiy, B.B., Zhou, H., et al. (2006). FSH directly regulates bone mass. Cell *125*, 247–260.

Suzawa, M., Takada, I., Yanagisawa, J., Ohtake, F., Ogawa, S., Yamauchi, T., Kadowaki, T., Takeuchi, Y., Shibuya, H., Gotoh, Y., et al. (2003). Cytokines suppress adipogenesis and PPAR-gamma function through the TAK1/TAB1/NIK cascade. Nat. Cell Biol. *5*, 224–230.

Syed, F., and Khosla, S. (2005). Mechanisms of sex steroid effects on bone. Biochem. Biophys. Res. Commun. *328*, 688–696.

Takeda, S., Elefteriou, F., Levasseur, R., Liu, X., Zhao, L., Parker, K.L., Armstrong, D., Ducy, P., and Karsenty, G. (2002). Leptin regulates bone formation via the sympathetic nervous system. Cell *111*, 305–317.

Takezawa, S., Yokoyama, A., Okada, M., Fujiki, R., Iriyama, A., Yanagi, Y., Ito, H., Takada, I., Kishimoto, M., Miyajima, A., et al. (2007). A cell cycle-dependent co-repressor mediates photoreceptor cell-specific nuclear receptor function. EMBO J. *26*, 764–774.

Teitelbaum, S.L. (2006). Osteoclasts; culprits in inflammatory osteolysis. Arthritis Res. Ther. *8*, 201.

Teitelbaum, S.L. (2007). Osteoclasts: what do they do and how do they do it? Am. J. Pathol. *170*, 427–435.

Teitelbaum, S.L., and Ross, F.P. (2003). Genetic regulation of osteoclast development and function. Nat. Rev. Genet. *4*, 638–649.

Tolar, J., Teitelbaum, S.L., and Orchard, P.J. (2004). Osteopetrosis. N. Engl. J. Med. *351*, 2839–2849.

Windahl, S.H., Andersson, G., and Gustafsson, J.A. (2002). Elucidation of estrogen receptor function in bone with the use of mouse models. Trends Endocrinol. Metab. *13*, 195–200.

Yoshizawa, T., Handa, Y., Uematsu, Y., Takeda, S., Sekine, K., Yoshihara, Y., Kawakami, T., Arioka, K., Sato, H., Uchiyama, Y., et al. (1997). Mice lacking the vitamin D receptor exhibit impaired bone formation, uterine hypoplasia and growth retardation after weaning. Nat. Genet. *16*, 391–396.

Zaman, G., Jessop, H.L., Muzylak, M., De Souza, R.L., Pitsillides, A.A., Price, J.S., and Lanyon, L.L. (2006). Osteocytes use estrogen receptor alpha to respond to strain but their ERalpha content is regulated by estrogen. J. Bone Miner. Res. *21*, 1297–1306.

Accession Numbers

Microarray can be seen in Gene Expression Omnibus under accession number GSE7798.

0090-9556/07/3510-1949–1955$20.00
DRUG METABOLISM AND DISPOSITION
Copyright © 2007 by The American Society for Pharmacology and Experimental Therapeutics
DMD 35:1949–1955, 2007

Vol. 35, No. 10
17327/3255799
Printed in U.S.A.

A Novel Mechanism for Polychlorinated Biphenyl-Induced Decrease in Serum Thyroxine Level in Rats

Yoshihisa Kato, Shin-ichi Ikushiro, Rie Takiguchi, Koichi Haraguchi, Nobuyuki Koga, Shinya Uchida, Toshiyuki Sakaki, Shizuo Yamada, Jun Kanno, and Masakuni Degawa

Kagawa School of Pharmaceutical Sciences, Tokushima Bunri University, Sanuki, Kagawa, Japan (Y.K.); Faculty of Engineering, Toyama Prefectural University, Toyama, Japan (S.I., T.S.); School of Pharmaceutical Sciences and Center of Excellence (COE) Program in the 21st Century, University of Shizuoka, Shizuoka, Japan (R.T., S.U., S.Y., M.D.); Daiichi College of Pharmaceutical Sciences, Fukuoka, Japan (K.H.); Faculty of Nutritional Sciences, Nakamura Gakuen University, Fukuoka, Japan (N.K.); and Division of Cellular & Molecular Toxicology, National Institute of Health Sciences, Tokyo, Japan (J.K.)

Received June 19, 2007; accepted July 12, 2007

ABSTRACT:

We have previously suggested that the decrease in the levels of serum total thyroxine (T_4) and free T_4 by a single administration to rats of Kanechlor-500 (KC500) at a dose of 100 mg/kg is not necessarily dependent on the increase in hepatic T_4-UDP-glucuronosyltransferase (UDP-GT). In the present study, we determined whether or not a consecutive treatment with KC500 at a relatively low dose (10 mg/kg i.p., once daily for 10 days) results in a decrease in the level of serum total T_4 and further investigated an exact mechanism for the KC500-induced decrease in the T_4. At 4 days after final treatment with KC500, the serum total T_4 and free T_4 levels were markedly decreased in both Wistar and UGT1A-deficient Wistar (Gunn) rats, whereas significant increases in hepatic T_4-UDP-GT activity were observed in Wistar rats but not in Gunn rats. The level of serum thyroid-stimulating hormone was not significantly changed in either Wistar or Gunn rats. Clearance from serum of the [^{125}I]T_4 administered to the KC500-pretreated Wistar and Gunn rats was faster than that to the corresponding control (KC500-untreated) rats. The accumulated level of [^{125}I]T_4 was increased in several tissues, especially the liver, in the KC500-pretreated rats. The present findings demonstrated that a consecutive treatment with KC500 resulted in a significant decrease in the level of serum total T_4 in both Wistar and Gunn rats and further indicated that the KC500-induced decrease would occur through increase in accumulation of T_4 in several tissues, especially the liver, rather than increase in hepatic T_4-UDP-GT activity.

Most polychlorinated biphenyls (PCBs) are known to decrease the level of serum thyroid hormone and to increase the activity of hepatic drug-metabolizing enzymes in rats (Van Birgelen et al., 1995; Craft et al., 2002). As possible mechanisms for the PCB-induced decrease in the level of serum thyroid hormone, enhancement of thyroid hormone metabolism by PCB and displacement of the hormone from serum transport proteins, including transthyretin (TTR), by PCB and its ring-hydroxylated metabolites are considered (Barter and Klaassen, 1992a, 1994; Brouwer et al., 1998). In particular, the decrease in the level of serum thyroxine (T_4) by 3,3′,4,4′,5-pentachlorobiphenyl, Aroclor 1254, and 2,3,7,8-tetrachlorodibenzo-*p*-dioxin in rats is believed to occur mainly through induction of the UDP-glucuronosyltransferases (UDP-GTs), especially UGT1A subfamily enzymes, responsible for glucuronidation of T_4 (Barter and Klaassen, 1994; Van Birgelen et al., 1995). However, the magnitude of decrease in the level of serum total T_4 is not necessarily correlated with that of increase in T_4-UDP-GT activity (Craft et al., 2002; Hood et al., 2003). Furthermore, we have reported that in Kanechlor-500 (KC500)-treated mice, serum T_4 level decreased without an increase in T_4-UDP-GT activity (Kato et al., 2003) and that the decrease in serum total T_4 level by a single administration of either KC500 or 2,2′,4,5,5′-pentachlorobiphenyl occurred even in UGT1A-deficient Wistar (Gunn) rats (Kato et al., 2004). Thus, an exact mechanism for the PCB-induced decrease in the level of serum thyroid hormone remains unclear. To date, most studies on biological effects of PCB have been performed using experimental animals treated once at a high dose (more than 100 mg/kg body weight), and the effect of the consecutive treatment at a low dose has been little reported. Humans and wild animals are exposed to a wide variety of environmental chemicals, including PCB, at a low level over a long period of time. Therefore, a study on biological effects by consecutive treatment with PCB at a low dose would be very important.

In the present study, therefore, we examined whether or not a consecutive treatment with KC500 at a relatively low dose (10 mg/kg i.p., once daily for 10 days) results in decrease in the level of serum total T_4 and further discussed a mechanism underlying the PCB-induced decrease in the T_4.

This work was supported in part by the Grant-in-Aid for Scientific Research (C) (no. 18510061; Y.K.) and for Scientific Research (B) (no. 19310042; K.H., Y.K.) from Japan Society for the Promotion of Science, and by a Health and Labour Sciences Research Grant for Research on Risk of Chemical Substances (H16-Kagaku-003; Y.K.) from the Ministry of Health, Labour and Welfare of Japan.

Article, publication date, and citation information can be found at http://dmd.aspetjournals.org.

doi:10.1124/dmd.107.017327.

ABBREVIATIONS: PCB, polychlorinated biphenyl; KC500, Kanechlor-500; T_3, triiodothyronine; T_4, thyroxine; TTR, transthyretin; TSH, thyroid-stimulating hormone; UDP-GT, UDP-glucuronosyltransferase.

Materials and Methods

Chemicals. Panacete 810 (medium-chain triglycerides) was purchased from Nippon Oils and Fats Co. Ltd. (Tokyo, Japan). The [^{125}I]T_4, radiolabeled at the 5'-position of the outer ring, was obtained from PerkinElmer Life and Analytical Sciences (Waltham, MA). The KC500 used in the present experiments contains 2,2',5,5'-tetrachlorobiphenyl (5.6% of total PCBs), 2,2',3,5',6-pentachlorobiphenyl (6.5%), 2,2',4,5,5'-pentachlorobiphenyl (10%), 2,3,3',4',6-pentachlorobiphenyl (7.4%), 2,3',4,4',5-pentachlorobiphenyl (7.7%), 2,2',3,4.4',5'-hexachlorobiphenyl (5.6%), and 2,2',4,4',5,5'-hexachlorobiphenyl (5.4%) as major PCB congeners (Haraguchi et al., 2005). All the other chemicals used herein were obtained commercially in appropriate grades of purity.

Animal Treatments. Male Wistar rats (160–200 g) and UGT1A-deficient Wistar rats (Gunn rats, 190–260 g) were obtained from Japan SLC., Inc. (Shizuoka, Japan). Male Wistar and Gunn rats were housed three or four per cage with free access to commercial chow and tap water, maintained on a 12-h dark/light cycle (8:00 AM to 8:00 PM light) in an air-controlled room (temperature, 24.5 ± 1°C; humidity, 55 ± 5%), and handled with human care under the guidelines of the University of Shizuoka (Shizuoka, Japan). Rats received consecutive intraperitoneal injections of KC500 (10 mg/kg) dissolved in Panacete 810 (5 ml/kg) at 24-h intervals for 10 days. Control animals were treated with vehicle alone (5 mg/kg).

In Vivo Study. Rats were killed by decapitation 4 days after the final administration of KC500. The liver was removed, and hepatic microsomes were prepared according to the method of Kato et al. (1995) and stored at −85°C until use. Blood was collected from each animal between 10:30 and 11:30 AM. After clotting at room temperature, serum was separated by centrifugation and stored at −50°C until use.

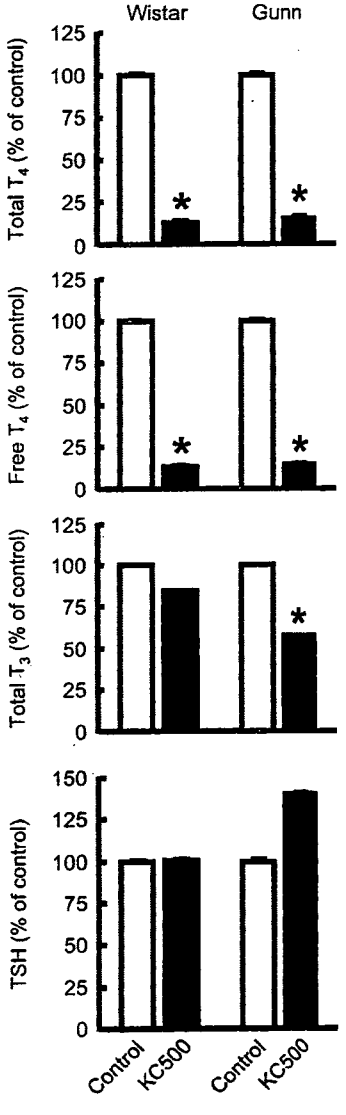

FIG. 1. Effects of KC500 on levels of serum total T_4, free T_4, total T_3, and TSH in Wistar and Gunn rats. Animals were killed 4 days after the final administration of KC500 (10 mg/kg i.p., once daily for 10 days), and levels of serum thyroid hormones were measured as described under *Materials and Methods*. Constitutive levels: total T_4, 4.29 ± 0.38 (Wistar, n = 5) and 5.80 ± 0.32 μg/dl (Gunn, n = 5); free T_4, 2.17 ± 0.16 (Wistar, n = 5) and 2.71 ± 0.17 ng/dl (Gunn, n = 5); total T_3, 0.34 ± 0.03 (Wistar, n = 6) and 0.96 ± 0.05 ng/ml (Gunn, n = 4); TSH, 4.89 ± 0.33 (Wistar, n = 5) and 7.48 ± 1.14 ng/ml (Gunn, n = 5). Each column represents the mean ± S.E. (vertical bars) for five to six animals. *, $P < 0.01$, significantly different from each control.

TABLE 1

Effects of KC500 on the activity of hepatic microsomal alkoxyresorufin O-dealkylases in Wistar and Gunn rats

Animals were killed at 4 days after the final administration of KC500 (10 mg/kg i.p., once daily for 10 days). The values shown are expressed as the mean ± S.E. for four to five animals.

Substrates	Wistar		Gunn	
	Control	KC500	Control	KC500
	nmol/mg protein/min		*nmol/mg protein/min*	
7-Benzyloxyresorufin	0.07 ± 0.01	3.34 ± 0.33*	0.03 ± 0.003	1.08 ± 0.27*
7-Pentoxyresorufin	0.03 ± 0.003	0.43 ± 0.05*	0.02 ± 0.003	0.22 ± 0.05*
7-Ethoxyresorufin	0.14 ± 0.01	9.02 ± 0.09*	0.21 ± 0.01	2.21 ± 0.29*

* $P < 0.05$, significantly different from each control.

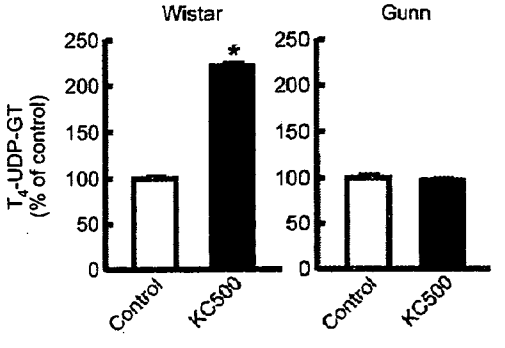

FIG. 2. Effects of KC500 on the activity of hepatic microsomal UDP-glucuronyltransferase in Wistar and Gunn rats. Each column represents the mean ± S.E. (vertical bars) for five to six animals. Constitutive levels: T_4-UDP-GT, 14.17 ± 1.11 pmol/mg protein/min (Wistar) and 6.36 ± 1.34 pmol/mg protein/min (Gunn). *, $P < 0.01$, significantly different from each control.

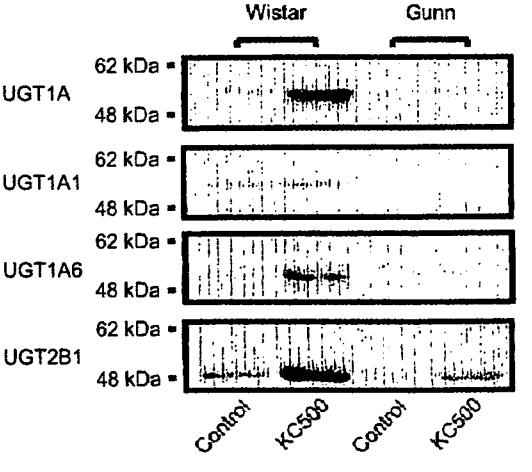

FIG. 3. Representative Western blot profiles for hepatic microsomal UGT isoforms in the KC500-treated Wistar and Gunn rats.

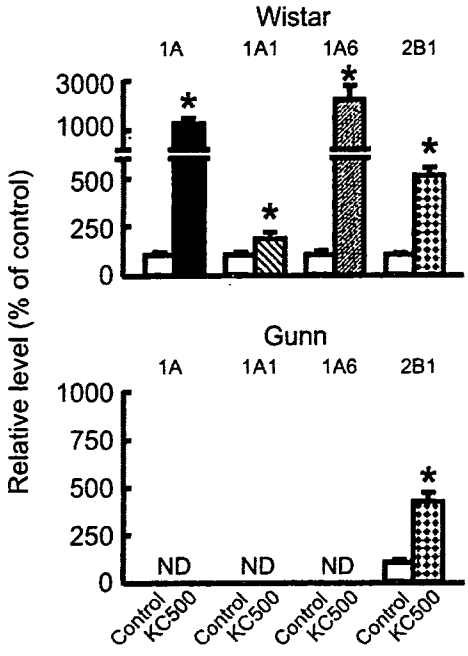

FIG. 4. Effects of KC500 on levels of hepatic microsomal UGT isoforms in Wistar and Gunn rats. The isolated bands responsible for UGT isoforms, which are shown in Fig. 3, were densitometrically quantified as described under *Materials and Methods*. The data are represented as the mean ± S.E. (vertical bars) for five to six animals. *, $P < 0.05$, significantly different from each control. ND, not detectable.

Analysis of serum hormones. Levels of total T_4, free T_4, total triiodothyronine (T_3), and thyroid-stimulating hormone (TSH) were measured by radioimmunoassay using Total T4 and Free T4 kits (Diagnostic Products Corporation, Los Angels, CA), the Triiodothyronine kit GammaCoat T_3 II (DiaSorin Inc., Stillwater, MN), and the rTSH [^{125}I] Biotrak assay system (GE Healthcare UK, Ltd., Little Chalfont, Buckinghamshire, UK), respectively.

Hepatic microsomal enzyme assays. Hepatic microsomal fraction was prepared according to the method described previously (Kato et al., 1995), and the amount of hepatic microsomal protein was determined by the method of Lowry et al. (1951) with bovine serum albumin as a standard. Microsomal *O*-dealkylase activities of 7-benzyloxy-, 7-ethoxy-, and 7-pentoxyresorufins were determined by the method of Burke et al. (1985).

Hepatic T_4-metabolizing enzyme assay. The activity of microsomal UDP-GT toward T_4 (T_4-UGT activity) was determined by the methods of Barter and Klaassen (1992b).

Western blot analysis. The polyclonal anti-peptide antibodies against the common region of UGT1A isoforms and specific antibodies against UGT1A1, UGT1A6, and UGT2B1, which were established by Ikushiro et al. (1995, 1997), were used. Western blot analyses for microsomal UGT isoforms were performed by the method of Luquita et al. (2001). The bands corresponding to UGT1A1, UGT1A6, and UGT2B1 on a sheet were detected using chemical luminescence (ECL detection kit; GE Healthcare UK, Ltd.), and the level of each protein was determined densitometrically with LAS-1000 (Fuji Photo Film. Co., Ltd., Tokyo, Japan).

Ex Vivo Study. At 4 days after a consecutive 10-day treatment with KC500, the rats were anesthetized with a saline (2 ml/kg) containing sodium pentobarbital (25 mg/ml) and potassium iodide (1 mg/ml). The femoral artery was cannulated (polyethylene tube SP31; Natsume Inc., Tokyo, Japan) and primed with heparinized saline (33 units/ml), and then the animal's body was warmed to 37°C. Fifteen minutes later, the rats were given i.v. 1 ml of [^{125}I]T_4 (15 μCi /ml) dissolved in the saline containing 10 mM NaOH and 1% normal rat serum.

Clearance of [^{125}I]T_4 from serum. The study on the clearance of [^{125}I]T_4 from serum was performed according to the method of Oppenheimer et al. (1968). In brief, after the administration of [^{125}I]T_4, a portion (0.3 ml) of blood was sampled from the artery at the indicated times, and serum was prepared and stored at −50°C until use. Two aliquots (15 μl each) were taken from each

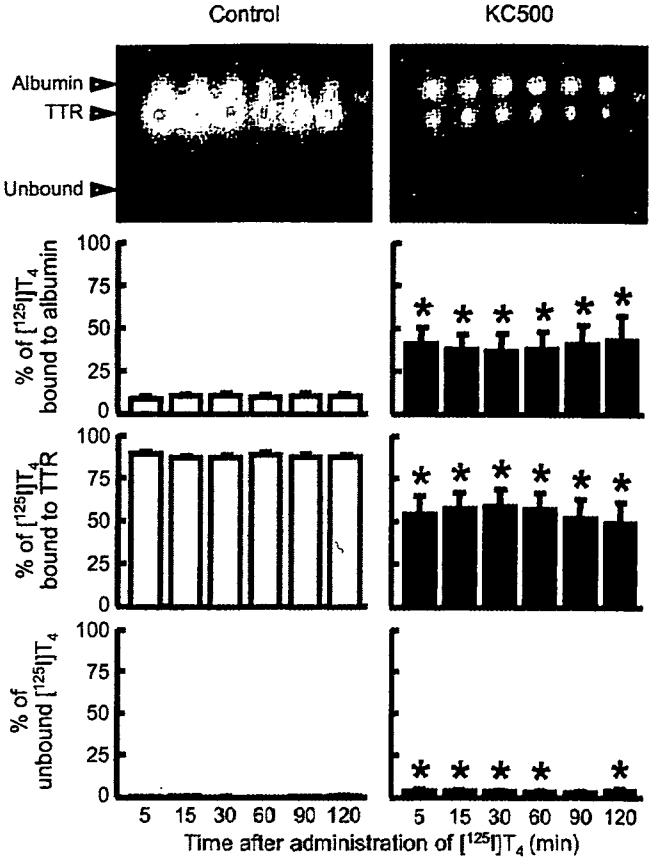

FIG. 5. Effects of KC500 on the binding of [^{125}I]T_4 to serum proteins in Wistar rats. Amounts of [^{125}I]T_4 bound to the serum proteins were assessed by the method described under *Materials and Methods*. Each column represents the mean ± S.E. (vertical bars) for three to six animals. *, $P < 0.05$, significantly different from each control.

serum sample for determining [^{125}I]T_4 level by a gamma counter (COBRA II AUTO-GAMMA 5002; PerkinElmer Life and Analytical Sciences).

Analysis of [^{125}I]T_4 bound to serum proteins. The levels of serum [^{125}I]T_4-albumin and [^{125}I]T_4-TTR complexes were determined according to the method of Davis et al. (1970). In brief, serum was diluted in 100 mM phosphate buffer (pH 7.4) containing 1 mM EDTA, 1 mM dithiothreitol, and 30% glycerol, and subjected to electrophoresis on 4 to 20% gradient native polyacrylamide gels PAG Mid "Daiichi" 4/20 (Daiichi Pure Chemicals Co., Ltd., Tokyo, Japan). The electrophoresis was performed at 4°C for 11 h at 20 mA in the 0.025 M Tris buffer (pH 8.4) containing 0.192 M glycine. The human albumin and TTR, which were incubated with [^{125}I]T_4, were also applied on the gel as templates. After the electrophoresis, a gel was dried and radioautographed for 20 h at room temperature using Imaging Plate 2040 (Fuji Photo Film Co., Ltd.). The levels of [^{125}I]T_4-albumin and [^{125}I]T_4-TTR in serum were determined by counting the gel fractions identified from Bio Imaging Analyzer (BAS-2000II IP Reader; Fuji Photo Film Co., Ltd.).

Tissue distribution of [^{125}I]T_4. The study on the tissue distribution of [^{125}I]T_4 was performed according to the modified method of Oppenheimer et al. (1968). In brief, at 60 min after administration of [^{125}I]T_4 to KC500-pretreated rats, blood was sampled from abdominal aorta. Then, cerebrum, cerebellum, pituitary gland, thyroid gland, sublingual gland, submandibular gland, thymus, heart, lung, liver, kidney, adrenal gland, spleen, pancreas, testis, prostate gland, seminal vesicle, stomach, duodenum, jejunum, ileum, cecum, brown fat, skeletal muscle, bone marrow, skin, spinal cord, and fat were removed and weighed. Radioactivities in serum and the tissues were determined by a gamma-counter (COBRA II AUTO-GAMMA5002; PerkinElmer Life and Analytical Sciences), and amounts of [^{125}I]T_4 in various tissues were shown as ratios of tissue to serum.

Statistics. The data obtained were statistically analyzed according to Stu-

dent's *t* test or Dunnett's test after analysis of variance. In addition, data of the clearance of [^{125}I]T_4 from serum and analysis of [^{125}I]T_4 bound to serum proteins were statistically analyzed according to the Newman-Keuls test after analysis of variance. The pharmacokinetic parameters of [^{125}I]T_4 were estimated with noncompartmental methods as described previously (Tabata et al., 1999).

Results

Serum Hormone Levels. Effects of KC500 on levels of serum thyroid hormones were examined in Wistar and Gunn rats (Fig. 1). In both Wistar and Gunn rats, KC500 treatment resulted in decreases of the serum total T_4 and free T_4, and the magnitude of the decrease in each serum thyroid hormone was almost the same in both strains of rats. On the other hand, a significant decrease in the level of serum total T_3 was observed in Gunn rats but not in Wistar rats. In addition, no significant change in TSH level was observed in either Wistar or Gunn rats.

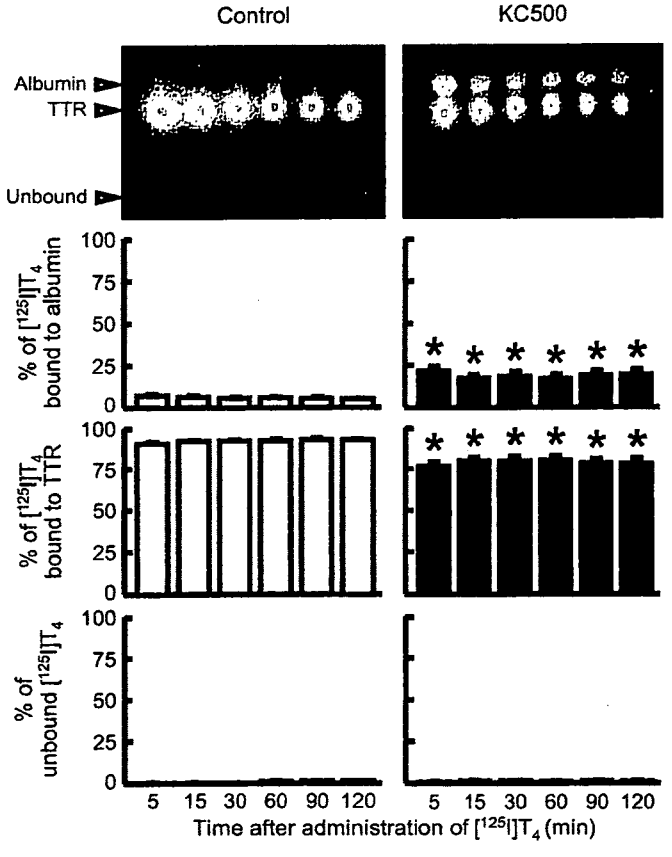

FIG. 6. Effects of KC500 on the binding of [^{125}I]T_4 to serum proteins in Gunn rats. Amounts of [^{125}I]T_4 bound to the serum proteins were assessed by the method described under *Materials and Methods*. Each column represents the mean ± S.E. (vertical bars) for four to five animals. *, $P < 0.05$, significantly different from each control.

Hepatic Drug-Metabolizing Enzymes. Effects of KC500 on hepatic microsomal activities of benzyloxyresorufin *O*-dealkylase (CYP2B1/2 and CYP3A1/2), pentoxyresorufin *O*-dealkylase (CYP2B1/2), and ethoxyresorufin *O*-dealkylase (CYP1A1/2) were examined in Wistar and Gunn rats. In both Wistar and Gunn rats, these enzyme activities were significantly increased by KC500 (Table 1), and the increase in each enzyme activity was much greater in Wistar rats than in Gunn rats.

Hepatic T_4-Metabolizing Enzyme Activities. T_4 glucuronidation is primarily mediated by hepatic T_4-UDP-GTs, such as UGT1A1 and UGT1A6, in the rat liver (Visser, 1996), and a chemical-mediated induction of the enzymes is considered to contribute to the decrease in the level of serum total T_4. Therefore, we examined effects of KC500 on hepatic microsomal T_4-UDP-GT activity in Wistar and Gunn rats. Constitutive activity of T_4-UDP-GT was approximately 2.2-fold higher in Wistar rats than in Gunn rats. Treatment with KC500 resulted in significant increase of T_4-UDP-GT activity in Wistar rats but not in Gunn rats (Fig. 2).

Western Blot Analysis for UGT1As. Levels of the proteins responsible for UGT1A enzymes, UGT1A1 and UGT1A6, were increased by KC500 treatment in Wistar rats but not in Gunn rats (Figs. 3 and 4). In addition, no expression of the UGT1A enzymes was confirmed in Gunn rats. On the other hand, the level of UGT2B1 was significantly increased by KC500 in both Wistar and Gunn rats, and magnitudes of the increase in both strains of rats were almost the same (Figs. 3 and 4).

Serum Proteins Bound to [^{125}I]T_4. The effects of KC500 on the binding of [^{125}I]T_4 to serum proteins, TTR, and albumin were examined in Wistar and Gunn rats (Figs. 5 and 6). In both Wistar and Gunn rats, pretreatment with KC500 resulted in a significant decrease in the level of [^{125}I]T_4-TTR complex, whereas it resulted in a significant increase in the level of [^{125}I]T_4 bound to albumin (Figs. 5 and 6).

Clearance of [^{125}I]T_4 from Serum. After an i.v. administration of [^{125}I]T_4 to the KC500-pretreated Wistar and Gunn rats, concentrations of [^{125}I]T_4 in sera were measured at the indicated times (Fig. 7). In both Wistar and Gunn rats, pretreatment with KC500 promoted the clearance of [^{125}I]T_4 from serum, and their serum [^{125}I]T_4 levels were decreased to approximately 40% of the initial level within 5 min. In the KC500-untreated Wistar and Gunn rats, serum [^{125}I]T_4 levels were gradually decreased to approximately 40% of the initial level at 120 min later. The serum pharmacokinetic parameters of the [^{125}I]T_4 estimated from these data (Fig. 7) were summarized in Table 2. The mean total body clearances (CL_{tb}) of [^{125}I]T_4 in the KC500-pretreated rats were 2.4 and 2.9 times, respectively, greater than those in the corresponding control rats. The steady-state volumes of distribution (Vd_{ss}) in the KC500-pretreated rats were 1.6 and 2.4 times, respectively, larger than those in the corresponding control rats.

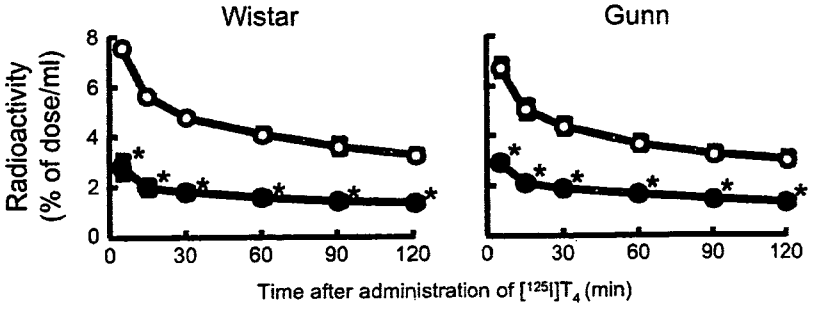

FIG. 7. Effects of KC500 on the clearance of [^{125}I]T_4 from serum in Wistar and Gunn rats. The amount of serum [^{125}I]T_4 was measured at the indicated times after the i.v. administration of [^{125}I]T_4. Each point represents the mean ± S.E. (vertical bars) for four to eight animals. *, $P < 0.001$, significantly different from each control. ○, control; ●, KC500.

Tissue Distribution of [^{125}I]T_4. The tissue-to-serum concentration ratio (K_p value) and distribution level of [^{125}I]T_4 in tissue after the administration of [^{125}I]T_4 to the KC500-pretreated Wistar and Gunn rats are shown in Figs. 8 and 9, respectively. K_p values of the thyroid gland and liver were the greatest among those of the tissues examined in either Wistar or Gunn rats (Fig. 8). In addition, K_p values in all the tissues examined, with the exception of the testis and ileum, were greater in KC500-pretreated Wistar rats than those in the corresponding control (KC500-untreated) rats. K_p values in the thyroid gland, liver, and jejunum in the KC500-pretreated Wistar and Gunn rats were 1.6 to 1.8, 3.3 to 3.8, and 4.7 to 11.5 times, respectively, higher than those in corresponding control rats (Fig. 8).

In the control Wistar and Gunn rats, the accumulation level of [^{125}I]T_4 was highest in the liver, among the tissues examined (Fig. 9). In both Wistar and Gunn rats, pretreatment with KC500 resulted in an increase in the accumulation level in the liver, and the levels increased to more than 40% of the [^{125}I]T_4 dosed (Fig. 9). Likewise, significant increase in accumulation of [^{125}I]T_4 was observed in the jejunum (Fig. 9). In addition, significant increases in the liver weight and accumulation level (per g liver) of [^{125}I]T_4 occurred in KC500-pretreated Wistar rats, but not in Gunn rats (Tables 3 and 4).

Discussion

In the present study, we found that consecutive treatment with KC500 (10 mg/kg i.p., once daily for 10 days; total dose, 100 mg/kg) promoted accumulation of T_4 in several tissues, especially the liver, and resulted in a drastic decrease in the levels of serum total T_4 and free T_4 in both Wistar and Gunn (UGT1A-deficient) rats. Thus, a decrease in the level of serum total T_4 is also observed in the Wistar and Gunn rats treated with KC500 (a single i.p. administration at a dose of 100 mg/kg) (Kato et al., 2004). In addition, constitutive levels of serum total T_4 and T_3 were higher in Gunn rats than in Wistar rats, and the results were identified with those as previously described by Benathan et al. (1983). The difference in constitutive level of serum thyroid hormone between Wistar and Gunn rats seems to be dependent on differences in the level and/or activity of T_4/T_3-UDP-GTs.

As a possible explanation for a chemical-induced decrease in serum thyroid hormones, a hepatic T_4-UDP-GT-dependent mechanism is generally considered, because T_4-UDP-GT inducers, including PCB, phenobarbital, 3-methylcholanthrene, pregnenolone-16α-carbonitrile, and clobazam, show strong activities for decreasing the level of serum total thyroid hormones, including T_4 and T_3 (Barter and Klaassen, 1994; Van Birgelen et al., 1995; Miyawaki et al., 2003). However, among the experimental animals treated with a T_4-UDP-GT inducer, the difference in magnitude of decrease in the level of serum total T_4 is not necessarily correlated with that of hepatic T_4-UDP-GT activity (Craft et al., 2002; Hood et al., 2003; Kato et al., 2003). Our present and previous results (Kato et al., 2004, 2005) using Wistar and Gunn rats support a hypothesis that significant decrease in the level of serum total thyroid hormones by either PCB or phenobarbital occurs primarily in a hepatic T_4-UDP-GT-independent pathway.

As a possible mechanism for the PCB-induced decrease in serum T_4 level, an increase in hepatic drug-metabolizing enzymes might be considered. However, these are induced to a greater extent in the Wistar rats than in the Gunn rats, whereas magnitudes of decrease in serum T_4 level in Wistar and Gunn rats were almost the same. Accordingly, the KC500-induced decrease in serum T_4 level is thought to be independent of the KC500-induced drug-metabolizing enzymes, including UDT-GTs and cytochromes P450.

As the factors regulating the level of serum total T_4, serum TSH, hepatic type I iodothyronine deiodinase, and TTR are known. However, no significant change in the level of serum TSH occurs in the PCB-treated rats (Liu et al., 1995; Hood et al., 1999; Hallgren et al., 2001; Kato et al., 2004). Hepatic type I iodothyronine deiodinase activity was significantly decreased in Wistar and Gunn rats by KC500 (Kato et al., 2004). On the other hand, a TTR-associated pathway might be considered as an explanation for the PCB-induced decrease in the level of serum total

TABLE 2

Pharmacokinetic parameters for [^{125}I]T_4 after the administration of [^{125}I]T_4 to the KC500-pretreated Wistar and Gunn rats

The experimental conditions were the same as those described in Fig. 7. The values shown are expressed as the mean ± S.E. for four to seven animals.

Animal	Treatment	Mean Total Body Clearance × 100	Distribution Volume
		ml/min	*ml*
Wistar	Control	7.82 ± 0.59	17.91 ± 0.52
	KC500	18.85 ± 3.49*	51.51 ± 6.34*
Gunn	Control	8.44 ± 0.22	20.21 ± 1.79
	KC500	13.84 ± 0.88*	48.91 ± 3.50*

* $P < 0.05$, significantly different from each control.

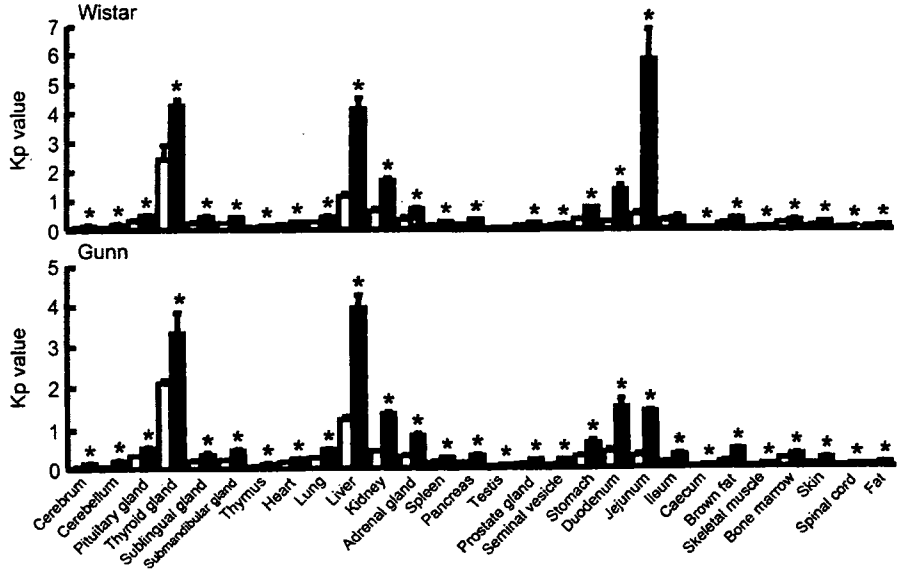

FIG. 8. Tissue-to-serum concentration ratio (K_p value) of [^{125}I]T_4 in various tissues after administration of [^{125}I]T_4 to the KC500-pretreated Wistar and Gunn rats. KC500 (10 mg/kg) was given i.p. to animals once daily for 10 days, and then, the animals were administered i.v. [^{125}I]T_4. At 60 min after administration of [^{125}I]T_4, the radioactivity in each tissue was measured. Each column represents the mean ± S.E. (vertical bars) for three to six animals. *, $P < 0.05$, significantly different from each control. □, control; ■, KC500.

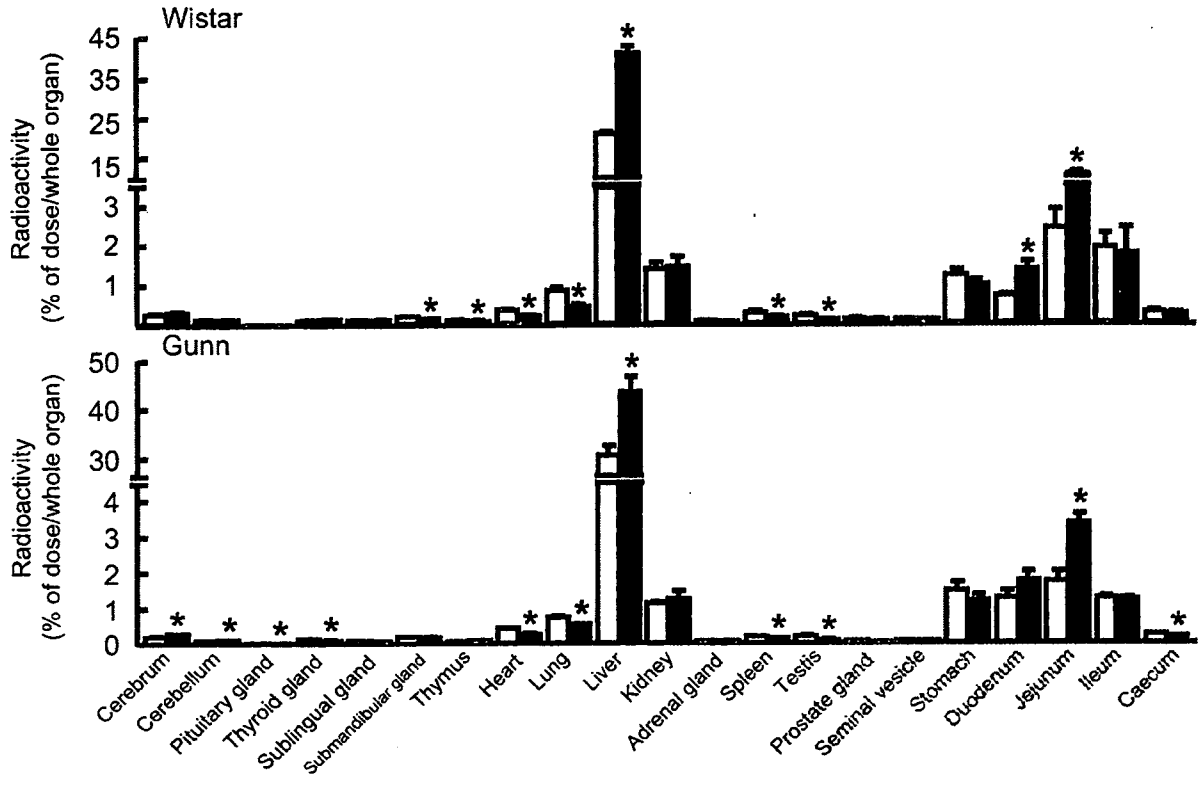

FIG. 9. Tissue distribution of [^{125}I]T_4 after administration of [^{125}I]T_4 to the KC500-pretreated Wistar and Gunn rats. The experimental conditions were the same as those described in Fig. 8. Each column represents the mean ± S.E. (vertical bars) for four to six animals. *, $P < 0.05$, significantly different from each control. □, control; ■, KC500.

TABLE 3

Liver weights after the administration of KC500 to Wistar and Gunn rats

Animals were killed at 4 days after the final administration of KC500 (10 mg/kg i.p., once daily for 10 days). The values shown are expressed as the mean ± S.E. for four to six animals.

Animal	Liver Weight	
	Control	KC500
	% of body weight	
Wistar	3.07 ± 0.04	3.81 ± 0.17*
Gunn	3.25 ± 0.08	3.38 ± 0.10

*$P < 0.01$, significantly different from each control.

TABLE 4

Accumulation of [^{125}I]T_4 in the KC500-pretreated Wistar and Gunn rat livers

The experimental conditions were the same as those described in Fig. 8. The values shown are expressed as the mean ± S.E. for four to six animals.

Animal	[^{125}I]T_4	
	Control	KC500
	% of dose/g liver	
Wistar	3.86 ± 0.18	6.01 ± 0.24*
Gunn	4.74 ± 0.43	6.33 ± 0.62

* $P < 0.001$, significantly different from each control.

T_4, because PCB and its ring-hydroxylated metabolites act as T_4 antagonists to TTR (Lans et al., 1993; Brouwer et al., 1998; Meerts et al., 2002; Kato et al., 2004). Thus, competitive inhibition by PCB and/or its metabolites would promote a decrease in the level of serum total T_4. In the present study, significant decrease in the level of [^{125}I]T_4 bound to serum TTR and increase in the level of [^{125}I]T_4 bound to serum albumin occurred in both KC500-pretreated Wistar and Gunn rats, suggesting that PCB and/or its metabolite(s) inhibit the formation of serum T_4-TTR complex.

Thus, inhibition of the T_4-TTR formation might lead to change in the tissue distribution of T_4. Therefore, to clarify this, we administered [^{125}I]T_4 to KC500-pretreated Wistar and Gunn rats and, thereafter, determined the levels of [^{125}I]T_4 in their tissues. In addition, since [^{125}I]T_4 in either plasma or tissues is known to be stable during 48 h (Oppenheimer et al., 1968), the radioactivity detected in the serum and tissues would be attributed to [^{125}I]T_4 in each tissue. Marked increases in the mean total body clearance of [^{125}I]T_4 and in the steady-state distribution volume of [^{125}I]T_4 were observed in the KC500-pretreated rats. A tissue-to-serum concentration ratio (K_p value) was greater in several tissues, especially the liver, of the KC500-pretreated Wistar and Gunn rats than in the corresponding control (KC500-untreated) rat tissues. In addition, in both KC500-pretreated Wistar and Gunn rats, more than 40% of the [^{125}I]T_4 dosed was accumulated in the liver.

In conclusion, the present findings confirmed that PCB-induced decrease in serum T_4 occurs not only in Wistar rats but also in Gunn (UGT1A-deficient) rats and further led to a hypothesis that the PCB-induced decrease occurs through increase in accumulation (transportation from serum to liver) of T_4 in the liver, rather than through induction of hepatic T_4-UDP-GT. In addition, the increased accumulation in the liver might be attributed to the PCB- and its metabolite(s)-mediated inhibition of formation of serum T_4-TTR complex.

References

Barter RA and Klaassen CD (1992a) UDP-glucuronosyltransferase inducers reduce thyroid hormone levels in rats by an extrathyroidal mechanism. *Toxicol Appl Pharmacol* **113**:36–42.
Barter RA and Klaassen CD (1992b) Rat liver microsomal UDP-glucuronosyltransferase activity

toward thyroxine: characterization, induction, and form specificity. *Toxicol Appl Pharmacol* **115**:261–267.

Barter RA and Klaassen CD (1994) Reduction of thyroid hormone levels and alteration of thyroid function by four representative UDP-glucuronosyltransferase inducers in rats. *Toxicol Appl Pharmacol* **128**:9–17.

Benathan M, Lemarchand-Beraud T, Berthier C, Gautier A, and Gardiol D (1983) Thyroid function in Gunn rats with genetically altered thyroid hormone catabolism. *Acta Endocrinol* **102**:71–79.

Brouwer A, Morse DC, Lans MC, Schuur AG, Murk AJ, Klasson-Wehler E, Bergman Å, and Visser TJ (1998) Interactions of persistent environmental organohalogens with the thyroid hormone system: mechanisms and possible consequences for animal and human health. *Toxicol Ind Health* **14**:59–84.

Burke MD, Thompson S, Elcombe CR, Halpert J, Haaparanta T, and Mayer RT (1985) Ethoxy-, pentoxy- and benzyloxyphenoxazones and homologues: a series of substrates to distinguish between different induced cytochromes P-450. *Biochem Pharmacol* **34**:3337–3345.

Craft ES, DeVito MJ, and Crofton KM (2002) Comparative responsiveness of hypothyroxinemia and hepatic enzyme induction in Long-Evans rats versus C57BL/6J mice exposed to TCDD-like and phenobarbital-like polychlorinated biphenyl congeners. *Toxicol Sci* **68**:372–380.

Davis PJ, Spaulding SW, and Gregerman RI (1970) The three thyroxine-binding proteins in rat serum: binding capacities and effects of binding inhibitors. *Endocrinology* **87**:978–986.

Hallgren S, Sinjari T, Håkansson H, and Darnerud PO (2001) Effects of polybrominated diphenyl ethers (PBDEs) and polychlorinated biphenyls (PCBs) on thyroid hormone and vitamin A levels in rats and mice. *Arch Toxicol* **75**:200–208.

Haraguchi K, Koga N, and Kato Y (2005) Comparative metabolism of polychlorinated biphenyls and tissue distribution of persistent metabolites in rats, hamsters, and guinea pigs. *Drug Metab Dispos* **33**:373–380.

Hood A, Allen ML, Liu Y, Liu J, and Klaassen CD (2003) Induction of T_4 UDP-GT activity, serum thyroid stimulating hormone, and thyroid follicular cell proliferation in mice treated with microsomal enzyme inducers. *Toxicol Appl Pharmacol* **188**:6–13.

Hood A, Hashmi R, and Klaassen CD (1999) Effects of microsomal enzyme inducers on thyroid-follicular cell proliferation, hyperplasia, and hypertrophy. *Toxicol Appl Pharmacol* **160**:163–170.

Ikushiro S, Emi Y, and Iyanagi T (1995) Identification and analysis of drug-responsive expression of UDP-glucuronosyltransferase family 1 (UGT1) isozyme in rat hepatic microsomes using anti-peptide antibodies. *Arch Biochem Biophys* **324**:267–272.

Ikushiro S, Emi Y, and Iyanagi T (1997) Protein-protein interactions between UDP-glucuronosyltransferase isozymes in rat hepatic microsomes. *Biochemistry* **36**:7154–7161.

Kato Y, Haraguchi K, Kawashima M, Yamada S, Masuda Y, and Kimura R (1995) Induction of hepatic microsomal drug-metabolizing enzymes by methylsulfonyl metabolites of polychlorinated biphenyl congeners in rats. *Chem-Biol Interact* **95**:257–268.

Kato Y, Haraguchi K, Yamazaki T, Ito Y, Miyajima S, Nemoto K, Koga N, Kimura R, and Degawa M (2003) Effects of polychlorinated biphenyls, Kanechlor-500, on serum thyroid hormone levels in rats and mice. *Toxicol Sci* **72**:235–241.

Kato Y, Ikushiro S, Haraguchi K, Yamazaki T, Ito Y, Suzuki H, Kimura R, Yamada S, Inoue T, and Degawa M (2004) A possible mechanism for decrease in serum thyroxine level by polychlorinated biphenyls in Wistar and Gunn rats. *Toxicol Sci* **81**:309–315.

Kato Y, Suzuki H, Ikushiro S, Yamada S, and Degawa M (2005) Decrease in serum thyroxine level by phenobarbital in rats is not necessarily dependent on increase in hepatic UDP-glucuronosyltransferase. *Drug Metab Dispos* **33**:1608–1612.

Lans MC, Klasson-Wehler E, Willemsen M, Meussen E, Safe S, and Brouwer A (1993) Structure-dependent, competitive interaction of hydroxy-polychlorobiphenyls, -dibenzo-*p*-dioxins and -dibenzofurans with human transthyretin. *Chem-Biol Interact* **88**:7–21.

Liu J, Liu Y, Barter RA, and Klaassen CD (1995) Alteration of thyroid homeostasis by UDP-glucuronosyltransferase inducers in rats: a dose-response study. *J Pharmacol Exp Ther* **273**:977–985.

Lowry OH, Rosebrough NJ, Farr AL, and Randall RJ (1951) Protein measurement with the Folin phenol reagent. *J Biol Chem* **193**:265–275.

Luquita MG, Catania VA, Pozzi EJS, Veggi LM, Hoffman T, Pellegrino JM, Ikushiro S, Emi Y, Iyanagi T, Vore M, and Mottino AD (2001) Molecular basis of perinatal changes in UDP-glucuronosyltransferase activity in maternal rat liver. *J Pharmacol Exp Ther* **298**:49–56.

Meerts IATM, Assink Y, Cenijn PH, van den Berg JHJ, Weijers BM, Bergman Å, Koeman JH, and Brouwer A (2002) Placental transfer of a hydroxylated polychlorinated biphenyl and effects on fetal and maternal thyroid hormone homeostasis in the rat. *Toxicol Sci* **68**:361–371.

Miyawaki I, Moriyasu M, Funabashi H, Yasuba M, and Matsuoka N (2003) Mechanism of clobazam-induced thyroidal oncogenesis in male rats. *Toxicol Lett* **145**:291–301.

Oppenheimer JH, Bernstein G, and Surks MI (1968) Increased thyroxine turnover and thyroidal function after stimulation of hepatocellular binding of thyroxine by phenobarbital. *J Clin Invest* **47**:1399–1406.

Tabata K, Yamaoka K, Kaibara A, Suzuki S, Terakawa M, and Hara T (1999) Moment analysis program available on Microsoft Excel®. *Xenobio Metab Dispos* **14**:286–293.

Van Birgelen APJM, Smit EA, Kampen IM, Groeneveld CN, Fase KM, van der Kolk J, Poiger H, van den Berg M, Koeman JH, and Brouwer A (1995) Subchronic effects of 2,3,7,8-TCDD or PCBs on thyroid hormone metabolism: use in risk assessment. *Eur J Pharmacol* **293**:77–85.

Visser TJ (1996) Pathways of thyroid hormone metabolism. *Acta Med Austriaca* **23**:10–16.

Address correspondence to: Dr. Yoshihisa Kato, Kagawa School of Pharmaceutical Sciences, Tokushima Bunri University, 1314-1, Shido, Sanuki, Kagawa 769-2193, Japan. E-mail: kato@kph.bunri-u.ac.jp

Arch Pharm Res Vol 30, No 4, 444-452, 2007

Archives of Pharmacal Research
http://apr.psk.or.kr

Gene Expression Profiles in T24 Human Bladder Carcinoma Cells by Inhibiting an L-type Amino Acid Transporter, LAT1

Shadi Baniasadi[1,2], Arthit Chairoungdua[2], Yuji Iribe[2], Yoshikatsu Kanai[2], Hitoshi Endou[2], Ken-ichi Aisaki[3], Katsuhide Igarashi[3], and Jun Kanno[3]

[1]National Research Institute of Tuberculosis and Lung Diseases, Shaheed Beheshti University of Medical Science, Tehran, Iran, [2]Department of Pharmacology and Toxicology, Kyorin University School of Medicine, 6-20-2 Shinkawa, Mitaka, Tokyo 181-8611, Japan, and [3]Division of Cellular & Molecular Toxicology, National Institute of Health Sciences, Kamiyoga 1-18-1, Setagaya-ku, Tokyo 158-8501, Japan

(Received November 13, 2006)

Inhibition of LAT1 (L-type amino acid transporter 1) activity in tumor cells could be effective in the inhibition of tumor cell growth by depriving tumor cells of essential amino acids. Because of the high level of expression of LAT1 in tumor cells, LAT1 inhibitors would be useful for anticancer therapy in suppressing tumor growth without affecting normal tissues. In recent years, cDNA microarray technique is useful technology for anticancer drug development. It allows identifying and characterizing new targets for developments in cancer drug therapy through the understanding genes involved in drug action. The present study was designed to investigate gene expression profile induced by LAT1 inhibitor using gene chip technology. Human bladder carcinoma cells (T24 cells) were treated with classical system L inhibitor 2-aminobicyclo-(2, 2, 1)-heptane-2-carboxylic acid (BCH). Gene chip experiment was applied for treated and untreated cells after 3 and 12 h. Two independent experiments with a high degree of concordance identified the altered expression of 151 and 200 genes after 3 and 12 h BCH treatment. Among these genes, 132 and 13 were up-regulated and 19 and 187 were down-regulated by 3 and 12 h BCH treatment respectively. We found that BCH affected the expression of a large number of genes that are related to the control of cell survival and physiologic behaviors. These data are useful for understanding of intracellular signaling of cell growth inhibition induced by LAT1 inhibitors as candidate for anticancer drug therapy.

Key words: BCH, Gene expression, Microarray, Bladder carcinoma cells, LAT1

INTRODUCTION

System L is a major nutrient transport system responsible for the Na^+-independent transport of large neutral amino acids including several essential amino acids (Christensen, 1990; Oxender and Christensen, 1963). In malignant tumors, a system L transporter L-type amino acid transporter 1 (LAT1) is up-regulated to support tumor cell growth (Kanai *et al.*, 1998; Sang *et al.*, 1995; Wolf *et al.*, 1996; Yanagida *et al.*, 2001) . It is proposed that the manipulation of system L activity, in particular that of LAT1, would have therapeutic implications. The inhibition of LAT1 activity in tumor cells could be effective in the inhibition of tumor cell growth by depriving tumor cells of essential amino acids (Kanai and Endou, 2001). Our previous studies have revealed that T24 cells express LAT1 in the plasma membrane together with its associating protein 4F2hc that inhibited by a system L-specific inhibitor 2-aminobicyclo-(2, 2, 1)-heptane-2-carboxylic acid (BCH) (Kim *et al.*, 2002; Yanagida *et al.*, 2001). An increased understanding of molecular mechanisms of LAT1 inhibitors will lead to the development LAT1 inhibitors for anticancer drug therapy.

cDNA microarray analysis permits the simultaneous and rapid analysis of the expression of tens of thousands of genes, and, in turn, provides an opportunity for determining the effects of anticancer agents. This technology will contribute to the more accurate development of therapeutic strategies and will help to determine the molecular mechanism(s) of action of chemopreventive and/or therapeutic agents (Li and Sarkar 2002; Macgregor and Squire,

Correspondence to: Shadi Baniasadi, National Research Institute of Tuberculosis and Lung Diseases Shaheed Beheshti University of Medical Science Tehran Iran
E-mail: sbaniasadi@yahoo.com, baniasadi@nrltld.ac.ir

2002). To better understand the precise molecular mechanisms by which BCH exerts its effects on T24 bladder carcinoma cells, we utilized a cDNA microarray to interrogate the mRNA levels of 39,000 genes and to determine the gene expression profiles of T24 bladder carcinoma cells treated with BCH.

MATERIALS AND METHODS

Cell culture and growth inhibition

T24 human bladder cancer cells were cultured in the growth medium (minimum essential medium supplemented with 10% fetal bovine serum) in a 5% CO_2 atmosphere at 37°C. For growth inhibition, 60 h after seeding (during logarithmic phase) T24 cells were treated with 20 mM BCH for 3 and 12 h.

cDNA microarray analysis for gene expression profiles

T24 cells were treated with 20 mM BCH for 3 and 12 h. The rationale for choosing these time points was to capture gene expression profiles of early response genes, genes that may be involved during the onset of growth inhibition. Total RNA from each sample was isolated by Trizol (Invitrogen) and purified by RNeasy Mini Kit and RNase-free DNase Set (QIAGEN, Valencia, CA) according to the manufactures' protocols. cDNA for each sample was synthesized by using Superscript cDNA Synthesis Kit (Invitrogen) using T7-(dT)24 primer instead of the oligo (dT) provided in the kit. The biotin-labeled cRNA was transcripted in vitro from cDNA using a BioArray HighYield RNA Transcript Labeling Kit (ENZO Biochem, New York, NY) and purified using an RNeasy Mini Kit. The purified cRNA was fragmented by incubation in fragmentation buffer (200 mmol/L Tris-acetate pH 8.1, 500 mmol/L KOAc, 150 mmol/L MgOAc) at 95°C for 35 min and chilled on ice. The fragmented labeled cRNA was applied to Human Genome U133 Array (Affymetrix, Santa Clara, CA), which contains 39,000 human gene cDNA probes, and hybridized to the probes in the array. After washing and staining, the arrays were scanned using a HP GeneArray Scanner (Hewlett-Packard, Palo Alto, CA). Two independent experiments were performed to verify the reproducibility of results.

Microarray data normalization and analysis

Data analysis was performed with the GeneChip Expression Analysis software (Affymetrix) and GeneSpring TM software (Silicon Genetics, Redwood, CA, U.S.A.). The differences in hybridization efficiency among arrays were equalized by intensities of spiked-in control mRNAs added to the sample in proportion to its DNA content (Kanno *et al.*, 2006). In a set of GeneChip experiments comparing the same sample hybridized to two different arrays, method-associated experimental artifacts produced less than two-fold differences between two identical samples. Thus, genes displayed over two-fold expression change were subjected to further testing. GeneChip array HG-U133A represents 22283 transcripts and the genes whose absolute call judged "present" in at least 1 sample were used for further analysis.

RESULTS

Cell growth inhibition by BCH treatment

Cell count showed that the treatment of T24 bladder cancer cells with BCH, time dependently inhibited cell proliferation (Fig. 1), demonstrating the growth inhibitory effect of BCH. These results are consistent with our previous study. This inhibition of cell proliferation could be due to altered regulation of gene expression by BCH.

Regulation of gene expression by BCH treatment

The gene expression profiles of T24 cells treated with BCH were assessed using cDNA microarray. Two inde-

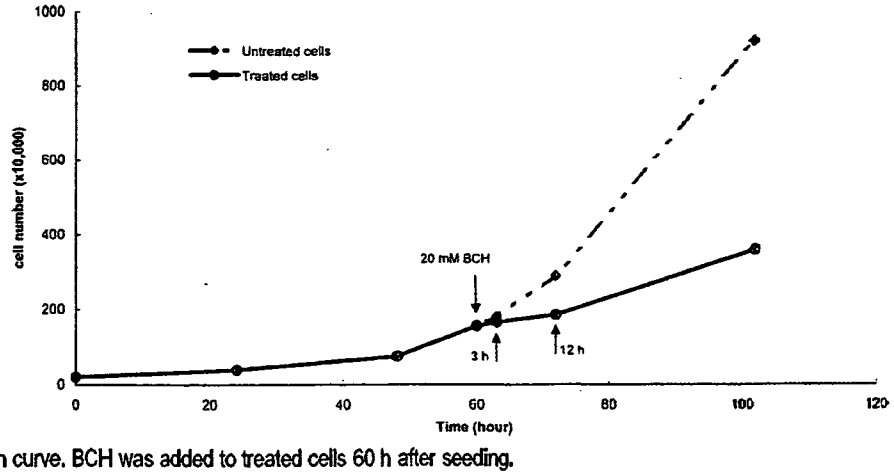

Fig. 1. T24 cell growth curve. BCH was added to treated cells 60 h after seeding.

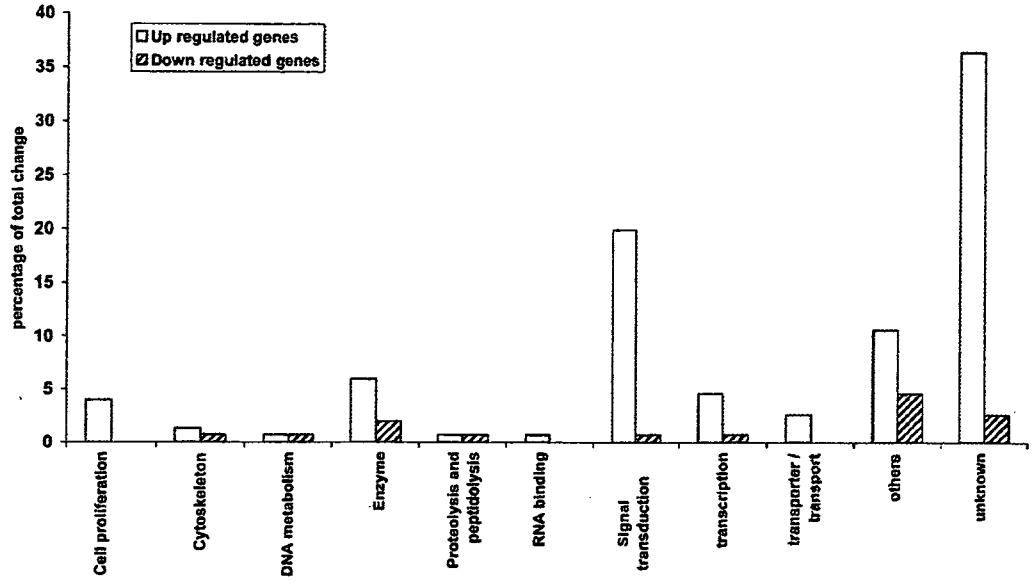

Fig. 2. Effect of BCH on gene expression after 3 h. Expression of many genes altered in T24 cells treated with BCH for 3 h.

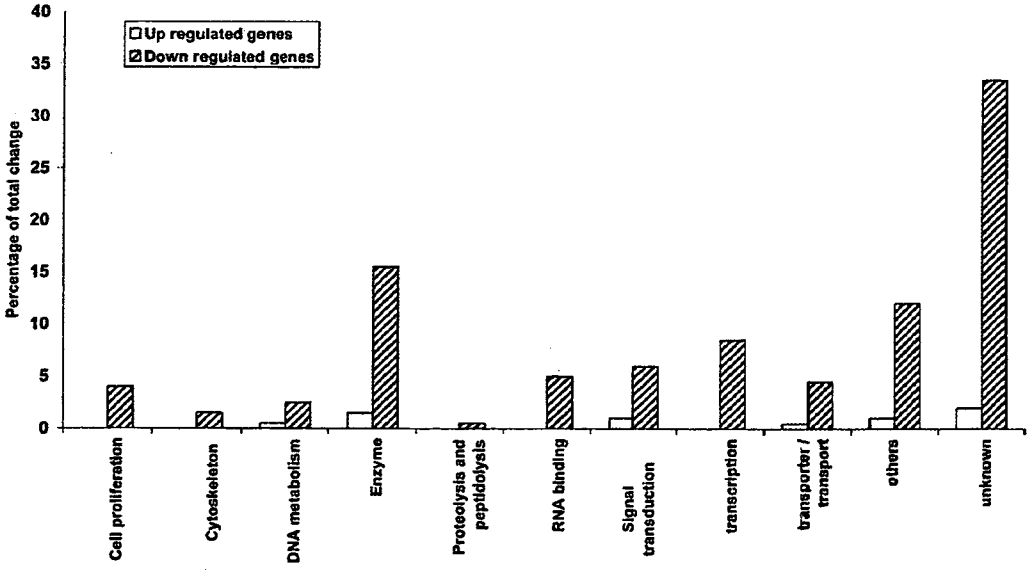

Fig 3. Effect of BCH on gene expression after 12 h. Expression of many genes altered in T24 cells treated with BCH for 12 h.

pendent experiments showed the altered expression of 151 and 200 genes at the mRNA level after 3 and 12 h BCH treatment. Among these genes, 132 and 13 were up-regulated and 19 and 187 were down-regulated by 3 and 12 h BCH treatment respectively. Expression of genes altered as early as 3 and 12 h of BCH treatment and was significantly up-regulated after 3 h and down-regulated after 12 h (Figs. 2 and 3). We found that after 3 h, BCH up-regulated genes that are involved mainly in signal transduction, enzyme reaction, transcription, cell proliferation and transport (Table I). On the other hand after 12 h, BCH down-regulated genes that are related mainly to enzyme reaction, transcription, signal transduction, RNA binding, transport, cell proliferation and DNA metabolism (Table II).

DISCUSSION

For continuous growth and proliferation, rapidly dividing tumor cells require more supply of sugars and amino acids. They are supported by the up regulation of transporters specialized for those nutrients. Transporters for essential amino acids are particularly important since they

Table I. Fold changes of specific genes in T24 cells treated with BCH for 3 h

genes	foldchange	t-test p-value
signal transduction		
Hypothetical protein	3.100	0.156
th79e05.x1 Soares_NhHMPu_S1 Homo sapiens cDNA clone IMAGE:2124896 3', mRNA sequence.	2.871	0.045
Sorting nexin 11	2.691	0.012
GABA(A) receptor-associated protein like 1	2.674	0.083
Down syndrome critical region gene 1	2.666	0.058
Interleukin 8	2.629	0.123
wd41c03.x1 Soares_NFL_T_GBC_S1 Homo sapiens cDNA clone IMAGE:2330692 3' similar to TR:O00538 O00538 F25B3.3 KINASE LIKE PROTEIN. ;, mRNA sequence.	2.596	0.439
Interleukin 8	2.534	0.087
IL2-inducible T-cell kinase	2.526	0.371
Protein kinase C, beta 1	2.427	0.151
Insulin-like growth factor binding protein 3	2.377	0.130
Vav 3 oncogene	2.267	0.053
Fibroblast growth factor 12B	2.237	0.127
CD53 antigen	2.216	0.106
MAD (mothers against decapentaplegic, Drosophila) homolog 7	2.194	0.073
GRO2 oncogene	2.186	0.020
G protein-coupled receptor 27	2.178	0.308
Adhesion glycoprotein	2.173	0.061
qq08e12.x1 Soares_NhHMPu_S1 Homo sapiens cDNA clone IMAGE:1931950 3', mRNA sequence.	2.159	0.027
Epiregulin	2.152	0.021
Gamma-aminobutyric acid (GABA) receptor, rho 2	2.143	0.159
DKFZP564L0862 protein	2.125	0.505
Insulin-like growth factor binding protein 1	2.080	0.216
GTP-binding protein overexpressed in skeletal muscle	2.074	0.056
Syntrophin, gamma 1	2.053	0.388
Adenosine A1 receptor	2.046	0.024
Inhibin, alpha	2.020	0.003
Frizzled (Drosophila) homolog 7	2.008	0.055
601763146F1 NIH_MGC_20 Homo sapiens cDNA clone IMAGE:4026010 5', mRNA sequence.	2.008	0.101
enzyme		
Cytosolic beta-glucosidase	2.668	0.209
UDP glycosyltransferase 1 family, polypeptide A1	2.355	0.014
wg36d09.x1 Soares_NSF_F8_9W_OT_PA_P_S1 Homo sapiens cDNA clone IMAGE:2367185 3', mRNA sequence.	2.287	0.072
Arginase, liver	2.201	0.339
Peptidylprolyl isomerase A (cyclophilin A)	2.166	0.423
ov13a06.x1 NCI_CGAP_Kid3 Homo sapiens cDNA clone IMAGE:1637170 3' similar to WP:R07B7.5 CE06267 ;, mRNA sequence.	2.116	0.270
cytochrome P450IIE1; Human cytochrome P450IIE1 (ethanol-inducible) gene, complete cds.	2.075	0.279
Keratin, hair, basic, 6 (monilethrix)	2.072	0.043
Protein kinase, Y-linked	2.028	0.430
transcription		
Homeo box A6	2.294	0.062
yf31g02.s1 Soares fetal liver spleen 1NFLS Homo sapiens cDNA clone IMAGE:128498 3', mRNA sequence.	2.024	0.259
Runt-related transcription factor 2	2.009	0.048